Evaluation of the Dynamic Core of the PALM Model System 6.0 in a Neutrally Stratified Urban Environment: Comparison between LES and Wind-tunnel Experiments

Tobias Gronemeier[1], Kerstin Surm[2], Frank Harms[2], Bernd Leitl[2], Björn Maronga[1,3], and Siegfried Raasch[1]

[1]Leibniz University Hannover, Institute of Meteorology and Climatology, Hannover, Germany
[2]Universität Hamburg, Meteorological Institute, Hamburg, Germany
[3]University of Bergen, Geophysical Institute, Bergen, Norway

Correspondence: Tobias Gronemeier (gronemeier@muk.uni-hannover.de)

Abstract. We demonstrate the capability of ~~PALM 6.0, the latest version of~~ the PALM model system ~~,~~ version 6.0 to simulate neutrally stratified urban boundary layers. ~~The studied scenario includes a real-case building setup~~ Our simulation uses the real-world building configuration of the HafenCity area in Hamburg, Germany. ~~Simulation results are evaluated against wind-tunnel measurements of the same building layout utilizing~~ Using PALM's virtual measurement module~~. The comparison reveals an overall very high agreement between simulation results and~~ , we compare simulation results to wind-tunnel measurements ~~not only for~~ of a down-scaled replica of the study area. Wind-tunnel measurements of mean wind speed ~~and direction but also for turbulence statistics~~ agree within $5\,\%$ on average while the wind direction deviates by approximately $4°$. Turbulence statistics similarly agree. However, larger differences between measurements and simulation arise ~~within close~~ in the vicinity of surfaces where ~~the resolution prevents good representation of the building layout. In the end~~building geometry is insufficiently resolved. We discuss how to minimize these differences by improving the grid layout and give hints for the setup preparation. Also, we discuss how ~~these differences can be reduced using already implemented~~ existing and upcoming features of PALM like the grid nesting and immersed boundary condition help to improve the simulation results.

1 Introduction

The PALM model system version 6.0 is the latest version of the ~~computational fluid-dynamics (CFD~~large-eddy simulation (LES) model PALM~~, a Fortran based codeto simulate~~ . PALM is a FORTRAN-based code, that simulates atmospheric and oceanic boundary layers. ~~Version~~ Development of the version 6.0 ~~was developed within the scope~~ followed the framework of the Urban Climate Under Change ([UC]^2) ~~framework~~ project, which is funded by the German Federal Ministry of Education and Research (Scherer et al., 2019; Maronga et al., 2019). ~~The aim of the~~ [UC]^2 ~~project is~~ aims to develop a fully functional urban climate model capable of simulating the urban canopy ~~layer from city scale down to building scale~~ with grid sizes down to $1\,\mathrm{m}$. ~~A~~ Maronga et al. (2015, 2020a) provide a detailed description of the ~~model system is given by Maronga et al. (2015, 2020a). PALM has already been applied in a variety of studies within the area of~~ PALM model system. A variety of urban boundary-

layer ~~research~~ studies have already used PALM successfully (e.g., Letzel et al., 2008; Park et al., 2012; Kanda et al., 2013; Kurppa et al., 2018; Wang and Ng, 2018; Paas et al., 2020). Built upon PALM version 4.0, the latest version, 6.0, contains many new features and improvements of ~~already existing components of~~ existing components in the model system. One of the most ~~impacting~~ impactful changes is the new treatment of surfaces within PALM. While previous versions of PALM did not distinguish between different surface types~~within former versions~~, it is now possible to directly specify a surface type to each individual solid surface within a model domain via the land-surface model (Maronga et al., 2020a) or the building surface model (Resler et al., 2017; Maronga et al., 2020a). Also, a fully three-dimensional obstacle representation is ~~possible while former~~ now possible. Previous versions allowed only a 2.5-dimensional representation of obstacles (no overhanging structures like bridges or gates). These additions ~~, however,~~ required extensive re-coding of ~~the former version~~ PALM 4.0, which affected ~~also~~ the dynamic core of the model. ~~This also includes~~ The re-coding included the modularization of the code base~~put further to practice~~, which lead to a re-ordering and re-grouping of code parts into several internal modules ~~like a~~ (e.g. constant flux-layer module, boundary-conditions module~~or~~ , turbulence-closure module, etc.). Changes to the dynamic core are ~~, however, limited to~~ technical changes, ~~i.e. the~~ only. The underlying physical equations ~~are still identical to the previous~~ in version 6.0 are identical to version 4.0.

~~Whereas former~~ Other studies evaluated previous versions of PALM ~~were already evaluated~~ against wind-tunnel measurements, real-world measurements ~~, and other CFD codes (Letzel et al., 2008; Razak et al., 2013; Park et al., 2015; Gronemeier and Sühring, , the significant changes of~~ and other computational fluid dynamics (CFD) codes (Letzel et al., 2008; Razak et al., 2013; Park et al., 2015; G . The significant changes to PALM's code base ~~produces~~ in version 6.0, however, produce different results compared to former versions. These ~~changes are either due to~~ differences are due to either round-off errors ~~purely because some code parts are not executed within the same order as before but may also be due to formerly unknown code defects being fixed or new defects being~~ or code defects. Round off-errors occur because the order of code execution differs from version 6.0 to 4.0. Old code defects may have been repaired when the dynamic core was modified, while new code defects may have been introduced. Hence, ~~the updated~~ version 6.0 requires a new evaluation~~from scratch. A sufficient evaluation is inevitable~~ , from scratch, to ensure confidence in the results of the PALM model system~~as it is also the case for every other CFD code (Blocken, 2015; Oberkampf et al., 2004).~~.

Because of the ~~high~~ complexity of PALM, evaluating the model is a ~~very~~ lengthy and costly exercise~~and a~~ . A complete validation of all model components would easily go beyond the scope of ~~any~~ a single article. ~~Within~~ In this study, we therefore focus ~~to evaluate~~ on the evaluation of the model's flow dynamics, which make up the core of the model system and build the foundation for all other features within PALM. ~~In order to isolate the pure~~ To isolate the dynamics from all other code parts, ~~PALM is operated~~ we operate PALM in a pure ~~dynamic~~ dynamic-driven mode, i.e. we switched off all thermal effects (temperature and humidity distribution, radiation, surface albedo, heat capacity, etc~~) are switched off. The simulation results can then be evaluated using~~ .). We can then compare the simulation results with wind-tunnel measurements ~~that are recorded in a similar setup as the simulation data as stated by~~ using the methodology of Leitl and Schatzmann (2010). While it is virtually impossible to neglect temperature or humidity effects in real-world measurements, wind-tunnel experiments can provide exactly the same idealized conditions as those used in our idealized simulation. ~~Also, other difficulties such as additional non-resolved~~

obstacles like trees or sub-grid features on building walls existing in the real world can make a comparison with real-world measurements troublesome (Paas et al., 2020). Paas et al. (2020) compared PALM simulations to measurements of a mobile measurement platform. Although they found overall good agreement was found between PALM and the measurements, some non-resolved obstacles like trees complicated the comparison at several points and led to differences in results. Hence, we decided to compare PALM against an idealized wind-tunnel experiment for this study.

A realistic building setup, in this case We use a real-world building configuration from the HafenCity area of Hamburg, Germany, is chosen for the study. , A real-case building setup has the advantage over more idealized, e.g. a single-cube, cases that a variety of different building configurations, also including more or less solitary buildings, can be covered in a single simulation. A real-case building setup has the advantage to is advantageous in that it can include a variety of building configurations, ranging from solitary buildings to complex street canyons, within a single simulation. Likewise, it may show the capability of PALM to correctly reproduce a complex, realistic wind distribution.

The evaluation study was originally designed We initially designed the evaluation study as a blind test where only the boundary conditions (building layout, approaching flow profile, location of measurements), but no further results of the wind-tunnel experiment was were available to conduct the PALM simulation. Such a blind test has the benefit to prevent of preventing model tuning and shows how well indicates how accurately a model can reproduce reference data only based on the based only on boundary conditions. This procedure also reflects a more realistic use case where reference data might not even exist. However, after comparing results from both PALM and wind-tunnel experiments, several errors within we identified several errors in the simulation setupwere identified like errors . Errors in building height and the roughness representation within the upwind region . The PALM setup was then updated were most prominent. We then updated the PALM setup with all identified flaws corrected and the case was re-simulated. Even though re-simulated the case. Although there are methods to adjust CFD results to better match to measurements (e.g., Blocken et al., 2007), these adjustments depend on the individual caseand need to , must be re-calculated for eachnew studied situation and are also only available , and are only usable if detailed reference data are available. Such setup tuning was not considered for the update of the We did not implement such setup tuning for the revised simulation setup. Corrections solely considered information that was already availableduring the first simulation but was just We made corrections solely to input parameters that were available, but not considered (layout of roughness elements within the wind tunnel) or simply incorrect (wrong not correct (incorrect building heights), during the initial blind-test simulation.

2 Experimental setup

2.1 Wind-tunnel experiment

Measurements were carried out We used measurements made at the Environmental Wind Tunnel Laboratory (EWTL) facility 'WOTAN' at the University of Hamburg, Germany. The $25\,\mathrm{m}$ long wind tunnel provides an $18\,\mathrm{m}$ long test section equipped with two turn tables and an adjustable ceiling. The cross section of the tunnel measures $4\,\mathrm{m}$ in width and $3\,\mathrm{m}$ in height. Figure 1 shows a photograph from within inside the wind tunnel for reference. For each wind tunnel wind-tunnel campaign, a neutrally stratified boundary layer flow is generated by a carefully optimized combination of turbulence generators at the inlet of the test

section, and a compatible floor roughness. For the present study, we modeled a boundary layer flow ~~was modelled~~ to match full scale conditions for a typical urban boundary layer measured at a $280\,\mathrm{m}$ tall tower in Billwerder, Hamburg. The mean wind profile ~~can be described by~~ fits a logarithmic wind profile with a roughness length $z_0 = (0.66 \pm 0.22)\,\mathrm{m}$ and ~~by~~ a power law with a profile exponent $\alpha = 0.21 \pm 0.02$. ~~The~~ Figure 2 depicts the approaching flow profile ~~is depicted in Fig. 2 and was modelled at a~~ for a modelled wind direction of $110°$.

~~An area of $2.6\,\mathrm{km}^2$ covering the HafenCityof~~ The miniature replica of the HafenCity, Hamburg, Germany ~~, was modelled at~~ has a scale of $m = 1/500$ ~~within the wind tunnel~~ and represents an area of $2.6\,\mathrm{km}^2$ (see Fig. 1). ~~Scaling of space l, time t and velocity u between~~ Standard quality measurements during the wind-tunnel experiment proved scale-independence of the results (based on Townsend's hypothesis of self similarity) and allowed scaling of the results from model scale (ms) ~~and~~ to full scale (fs)~~is then~~ . Scaling of space l, time t and velocity u is achieved via

$$l_{\mathrm{fs}} = \frac{l_{\mathrm{ms}}}{m}, \tag{1}$$

$$t_{\mathrm{fs}} = \frac{t_{\mathrm{ms}}}{m}, \tag{2}$$

$$u_{\mathrm{fs}} = u_{\mathrm{ms}}. \tag{3}$$

~~A~~ We used a 2D Laser-Doppler-Anemometry (LDA) System ~~was used~~ to measure component-resolved flow data at sampling rates of $200\,\mathrm{Hz} - 800\,\mathrm{Hz}$ (model scale)~~, resolving~~ . This measurement method resolves even small-scale turbulence in time at most ~~but unfortunately not all~~ measurement locations. ~~At each measurement location a 3 minutes time series was recorded~~We recorded a three-minute time series at each measurement location, which corresponds to a period of about 25 hours at full scale. ~~The~~ Prandtl tubes continuously monitored the reference wind speed ~~was permanently monitored~~ close to the tunnel inlet~~through Prandtl tube measurements~~. For the model evaluation case presented here, measurements were taken at 25 different locations within the building setup as shown in Fig. 3. As the measurements were originally planned and used for a different study focusing on near-ground ventilation and pedestrian wind comfort, locations were not specifically chosen for the present study. However, the measurements still cover ~~different~~ a variety of aspects of the flow within the building canopy including open areas, narrow and wide street canyons as well as intersections.

2.2 PALM simulation

~~The~~ We used the PALM Model System 6.0, revision 3921, ~~was used~~ to conduct the simulation for this study. ~~PALM was operated~~ We operated PALM using a fifth-order advection scheme after Wicker and Skamarock (2002) in combination with a third-order Runge-Kutta time-stepping scheme after Williamson (1980). ~~At this point, we skip~~ Maronga et al. (2015, 2020a) provide a detailed description of the PALM model~~, which is provided by Maronga et al. (2015, 2020a). The simulation was conducted~~ . We conducted the simulation at full scale with a domain ~~covering an area~~ size of $6000\,\mathrm{m}$ by $2880\,\mathrm{m}$ horizontally and $601\,\mathrm{m}$ vertically at a ~~spacial~~ spatial resolution of $\Delta x = \Delta y = \Delta z = 1\,\mathrm{m}$ in each direction. This ~~resulted in about~~ domain resulted in approximately 10.4×10^9 grid points ~~for the used staggered Arakawa C~~ in our staggered Arakawa-C grid (Harlow and Welch, 1965; Arakawa and Lamb, 1977). The ~~area of interest~~study region, i.e. the HafenCity area, was situated downstream

of the simulation domain. ~~The model domain was oriented so that~~ We aligned the mean flow direction ~~was aligned~~ with the x-direction. ~~With a mean wind direction of 110°,~~ Hence, we rotated the model domain ~~was hence rotated counter-clockwise~~ counter clockwise by 200° to produce a mean wind direction of 110°.

~~The building layout as~~ Figure 4 displays the building layout used in PALM~~is depicted in Fig. 4. In PALM , topography is considered using~~ . PALM uses the mask method (Briscolini and Santangelo, 1989) for topography, where a grid volume is either 100 % fluid or 100 % obstacle. In combination with PALM's rectilinear grid, this ~~can cause buildings not aligned with the grid to appear differently, more brick-like, than they were within the wind tunnel~~method can cause non-grid aligned buildings to have inconsistent geometries (step-like) when compared with the wind-tunnel replica.

~~The basic~~ We based the setup for this study ~~is based~~ on the settings used ~~in the former study of Letzel et al. (2012).~~ by Letzel et al. (2012). A heterogeneous building setup usually requires a non-cyclic boundary condition along the mean flow direction to ensure that building-induced turbulence is not ~~cycled over and over~~ recycled into the analysis area~~which otherwise might influence the results~~. However, tests with non-cyclic boundary conditions along the mean flow showed that simulations would require extremely long simulation times ~~would be required~~ to generate a stationary state. Hence, we used cyclic boundary conditions instead, which reduced the required CPU-time significantly. ~~The domain was extended~~ We extended the domain in mean flow direction (x-direction) to allow the building-induced turbulence to dissipate before the flow hits the target area again due to the cyclic conditions. ~~As the simulation was aimed at a pure neutral case and without releasing any~~ Because we simulated an ideal, neutrally-stratified case that neglected trace gases or alike within the city area, there was no disadvantage ~~in using~~ to use cyclic boundary conditions~~instead~~. After a simulation time of 1.5 hours~~steady-state conditions were reached~~ , the simulation reached a steady state.

~~A~~ We assumed a constant flux layer ~~was assumed~~ between the surface and the first computational grid level to calculate the surface shear stress. The exact value of the roughness length, z_0, for the building surfaces is not known from the wind-tunnel experiment. Therefore, it was estimated as $z_0 = 0.01\,\mathrm{m}$~~which also satisfied the general recommendation~~ , This value was recommended by Basu and Lacser (2017) who state $z_0 \leq 0.02 \cdot \min(\Delta z)$. Due to the staggered grid, the first computational level was positioned $0.5\Delta z$ above the surface~~, hence~~. Hence, $z_0 = 0.02 \cdot 0.5 \cdot 1\,\mathrm{m} = 0.01\,\mathrm{m}$.

~~For~~ The estimated roughness length of the approaching flow ~~, the modelled roughness length was estimated as $z_0 = (0.66 \pm 0.22)\,\mathrm{m}$ within~~ in the wind-tunnel experiment ~~(cf.~~ was $z_0 = (0.66 \pm 0.22)\,\mathrm{m}$ (see Sect. 2.1). ~~With the chosen resolution of 1 m such large roughness cannot be represented by be used surface-flux parameterization, but needs to be explicitly simulated by resolved-scale roughness elements . They were placed within the simulation domain~~ Surface-flux parameterizations cannot represent such a large roughness length at the simulated resolution (1 m). Therefore, we explicitly resolved the roughness using roughness elements of the exact same shape and layout as ~~they were present~~ those elements used in the wind-tunnel experiment. This ~~produced a similar~~ methodology produced a boundary layer flow ~~within both experiments as shown in Fig. 2~~in the simulation similar to that observed in the wind-tunnel experiment (see Fig. 2).

To match the conditions within the wind tunnel, we considered a strictly neutral atmosphere ~~was considered~~ with potential temperature being constant over time. ~~Also,~~ We also neglected the Coriolis force~~was neglected~~.

In the past, Munters et al. (2016) reported persistent streak-like structures artifacts in the flow field, that are oriented along the mean-wind directionwere reported , for LES of neutral flows using cyclic boundary conditions(Munters et al., 2016). Such streaks naturally develop within the neutral boundary layerand , reach lengths of several kilometres, and move along the mean wind direction while not moving in mean-wind direction while remaining stationary in the span-wise direction. They These streaks form randomly and have a limited lifetime. In combination with cyclic boundary conditions, however, the start and end of a streak can merge, forming an infinite streak that is self-containing and persistent in time. To avoid the artificial persistence of these structures by cyclic boundary conditions, a shifting method was used according to we use the shifting method of Munters et al. (2016). This method breaks up the infinite and persistent streak-like structures artifacts and ensures a natural dissipation. The flow was shifted We shifted the flow by $300\,\mathrm{m}$ in y-direction, i.e. perpendicular to the mean wind mean-wind direction, before entering the domain at the left boundary.

The wind field was initialized using initializes with a turbulent wind field from a precursor simulation via the cyclic-fill method (Maronga et al., 2015). The setup of the precursor simulation was similar to the main simulation but with a reduced domain size of $600\,\mathrm{m}$ by $600\,\mathrm{m}$ in horizontal direction. To initialize the precursor simulation, we measured the normalized approaching wind profile as measured in the wind tunnel was used and scaled to a wind speed of and scaled the wind speed to $4\,\mathrm{m\,s^{-1}}$ at $50\,\mathrm{m}$ height to get obtain a representative wind speed for within the canopy layer. This resulted in a The fixed wind speed of was $6.26\,\mathrm{m\,s^{-1}}$ at the top boundary for the precursor and main simulation.

The total simulation time of the main simulation was 4 hoursof which . The simulation achieved a steady state after the first 1.5 hourswere required to reach a steady state of the simulation. The . We used the results from the final 2.5 hours were used for the analysis presented here (see Sect. 3).

Figure 2 shows the mean wind profile of the flow approaching the building area during the analysis time, as well as the approaching flow of the wind-tunnel experiment. Note that we defined the street-level height is defined as at $z = 0\,\mathrm{m}$while , and the lower-most height was at water level, which is $5\,\mathrm{m}$ below street level (cf. see Fig. 4). Hence, the shown approaching wind profile shown in Figure 2 starts at $z = -5\,\mathrm{m}$.

2.3 Measurement stations

Within the wind-tunnel experiment, wind speed was measured at certain measurement stations within the building array. The locations of which are shown in Fig. 3 Figure 3 shows the locations of the measurement stations. To be able to mirror the measurements as best as possible, we used the virtual measurement module of PALM was used (Maronga et al., 2020a). This module allows to define defines several virtual measurement stations within the model domain via geographical coordinates. The model domain itself then needs to must be geo-referenced in order to identify the grid points closest to the measurement location. Referencing is done by assigning geographical coordinates and orientation to PALM references the geographical coordinates based on the coordinates of the lower left corner of the domain and the domain's orientation.

When mapping the measurement stations onto the PALM grid, there were two difficulties: First, there was not always a grid point available at the exact location of the measurement within the wind-tunnel experiment. Therefore, measurement positions are slightly shifted between both experiments can differ between the virtual and wind-tunnel measurements by a distance of

less than 1 m. Second, the topography in ~~close~~ the vicinity of a measurement point ~~might have been slightly different due to~~ at the virtual stations may differ from the wind-tunnel stations due to the topography representation used in PALM (see Sect. 2.2). To overcome these two issues, ~~virtual measurements not only from the closest grid point to~~ we recorded virtual measurements also from the grid points neighbouring a measurement position~~were saved but also values from the neighbouring grid points~~. In post-processing, we analyzed the area of each measurement station ~~was analyzed and a grid point selected that best fitted~~ and selected the measurement from the grid point that best fit the wind-tunnel measurements.

~~At each measurement station presented in this study, vertical profiles were recorded~~ Each measurement station recorded vertical profiles with a sampling rate between ~~8.7 Hz – 11.2 Hz~~ 8.7 Hz – 11.2 Hz (measurements recorded during each time step).

3 Results

3.1 PALM simulation

The PALM simulation required a spin-up time of 1.5 hours~~as can be seen~~, which is evident by the time series of the domain-averaged kinetic energy $E = 0.5\sqrt{u^2 + v^2 + w^2}$ and the friction velocity u_* (see Fig. 5). Both quantities stabilized after 1.5 hours at ~~around~~ approximately $E = 15.4\,\mathrm{m^2\,s^{-2}}$ and $u_* = 0.16\,\mathrm{ms^{-1}}$. Therefore, we evaluated only data from the last 2.5 hours of the simulation~~were used for the following evaluation~~.

~~The~~ Figure 6 shows the horizontally and time-averaged vertical profile of the stream-wise component of the vertical momentum flux wu~~is shown in Fig. 6~~. The vertical momentum flux wu ~~can be~~ is split into a resolved component and a sub-grid scale (SGS) ~~part which is parameterized via an SGS model . The higher the resolved part, the~~ component. An SGS model parameterizes the SGS component. The less the SGS model contributes to the flux ~~therefore indicating that the flux and hence~~ the better resolved is the turbulence causing the flux~~is well resolved~~. The ratio of the resolved and the total momentum flux ~~(total meaning resolved plus SGS part)~~ is close to 1 revealing that ~~turbulence is properly resolved within~~ the simulation domain properly resolved the turbulence (see Fig. 6). ~~At the surface, turbulence is less resolved due to the fact that turbulent~~

Turbulent structures tend to become smaller the closer they get to the surface~~and cannot be resolved by the grid spacing any more~~. Hence, at the surface, the constant grid spacing resolves less turbulence (Maronga et al., 2020b). However, the ratio between resolved and total wu ~~is above~~ exceeds 0.9 except for the lowest two grid levels, where the ratio ~~drops down~~ reduces to 0.78. The ~~small disturbance that is visible~~ discontinuity at $z = 15\,\mathrm{m}$ is related to the roughness elements. Most of these elements ~~reach up until~~ extend to $z = 15\,\mathrm{m}$, causing the disturbance in the vertical wu profile at that height.

To ~~get an impression of~~ visualize the turbulent structures, ~~Fig.~~Figure 7 shows a snapshot of the magnitude of the three-dimensional vorticity as a ~~measure of turbulence. One can clearly identify strong turbulent features~~ proxy for turbulence. Strong turbulence (yellow and red structures) ~~within~~ occurs in the vicinity of buildings~~while only weak turbulence is present~~, while weak turbulence occurs above smooth surfaces. ~~Strong turbulence outside of the building array is caused by roughness~~ Roughness elements that are not visible within ~~the figure~~Figure 7 cause the strong turbulence outside of the building array.

3.2 Comparison between ~~wind-tunnel~~ wind tunnel and PALM

To compare ~~both experiments, results must be normalized first as the experiments~~ the simulation and the wind-tunnel experiment, we must first normalize the results as the simulation and wind-tunnel experiment were conducted on different scales and ~~used different~~ mean wind speeds. The reference wind speed u_{ref} used for normalization corresponds to the wind speed of the approaching flow at a height of $50\,\mathrm{m}$ (full scale). ~~The reference height was defined by previously~~ Previously conducted laboratory experiments defined the reference height to be representative ~~for~~ of the measured canopy flow~~and is expected to be well within the height range for that~~. The reference height falls within the range expected to most accurately model a scaled neutrally-stratified atmospheric boundary layer wind flow~~could be modeled most accurately. In the following, results are given~~. We report our results at full scale ~~if not stated otherwise~~ unless otherwise stated.

Figure 8 shows the wind distribution for each measurement station at the lowest measurement height for (a) the wind-tunnel measurements ($z = 3\,\mathrm{m}$) and (b) the PALM simulation ($z = 2.5\,\mathrm{m}$). Due to the staggered grid used in PALM (~~cf.~~ see Sect. 2.2), the positions of the PALM measurements are ~~positioned~~ $0.5\,\mathrm{m}$ below their corresponding wind-tunnel measurements. Note, that measurement station 15 ~~(cf. Fig. 3) was positioned~~ stands on top of a building where measurements were only available above $18\,\mathrm{m}$ height (see Fig. 3). At most measurement stations, the main wind direction ~~is similar~~ in the PALM simulation ~~compared~~ is similar to the wind-tunnel data.

~~Noticeable differences of the wind distribution~~ Noticeable differences in the distribution of wind directions occur at stations 6, 7, 10, and 20, where the PALM simulation reports a larger variation in wind ~~direction~~ directions or a different mean wind direction~~is reported within the PALM simulation~~. On average, wind speed is ~~about~~ $9\,\%$ less in the PALM simulation ~~compared to~~ than in the wind-tunnel measurements.

At ~~the next measurement height (wind tunnel: 10 m;~~ $10\,\mathrm{m}$ height (PALM: $9.5\,\mathrm{m}$), the wind ~~distribution is~~ distributions are still very close between PALM and the wind tunnel at most stations (see Fig. 9). Stations 6, 10 and 20 still show noticeable differences. The difference in average wind speed reduces to $5\,\%$ between PALM and wind-tunnel results. ~~This~~ At $40\,\mathrm{m}$ height and above, the difference reduces to less than $2.5\,\%$~~at 40 m height and above~~.

~~A more detailed comparison of the difference in wind speed is given by Fig. 10 which~~ Figure 10 shows scatter plots of wind-tunnel and PALM measurements at each station and height, which are 173 data pairs in total. Looking at the horizontal wind speed U_{hor} and the wind-speed components u and v, PALM underestimates the lower ~~wind speeds while higher wind speeds~~ values while higher values compare well to the wind-tunnel measurements. Wind direction d differs by less than $4°$ on average with a maximum difference of less than $44°$. It has to be noted, however, that ~~wind tunnel~~ wind-tunnel measurements might be located between grid points of the PALM grid creating a ~~spacial~~ spatial offset between the measurements. Especially close to obstacles, this ~~spacial~~ spatial offset can lead to differences between both experiments.

~~The~~ Three major reasons caused the general lower wind ~~speed recorded within PALM has three major reasons~~speeds in the PALM simulation: (i) a miss-match in measurement height, (ii) a miss-match in z_0 between both experiments and (iii) the step-wise building representation caused by PALM's rectilinear grid. ~~Within PALM , measurements were~~ The staggered Arakawa-C grid caused the PALM measurements to be located $0.5\,\mathrm{m}$ ~~lower than in the~~ below the corresponding wind-tunnel

~~experiment due to the staggered Arakawa C grid (~~measurements. PALM calculates u and v ~~values are calculated~~ at half the height of each grid cell~~; given that~~ . With a grid size of $\Delta z = 1\,\mathrm{m}$, u and v are~~hence~~ , hence, calculated at heights of $0.5\,\mathrm{m}$, $1.5\,\mathrm{m}$, $2.5\,\mathrm{m}$, ~~and so on) and were not interpolated to different heights~~ etc. We chose to not interpolate between the height levels in order to not alter the simulation results by adding additional uncertainty due to the chosen interpolation techniques. When comparing PALM results at $0.5\,\mathrm{m}$ above the wind-tunnel measurements, the underestimation of wind-speed reduces to $5\,\%$ at $3\,\mathrm{m}$ height. Because vertical gradients of the wind-speed decrease with height, differences in measurement heights are less severe at greater heights.

Second, a miss-match of z_0 between both experiments ~~also~~ affects results most significantly also at the lowest height levels. This is supported by the fact that we observed the largest difference in mean wind speed ($9\,\%$ lower wind speed) ~~is observed~~ at the lowest measurement height. Hence, the surfaces ~~within~~ in the wind-tunnel experiment might have been smoother than estimated~~for the PALM simulation~~ , and $z_0 = 0.01\,\mathrm{m}$ might have been too large. ~~However, in~~ In a different not yet published wind-tunnel experiment with similar wall materials of the building model, ~~roughness lengths were observed~~ we observed roughness lengths between $0.002\,\mathrm{m}$ and $0.01\,\mathrm{m}$. This puts the chosen z_0 for the simulation at the upper end of the possible value range for the roughness within the wind-tunnel experiment.

The third reason, the step-wise building representation, affects results within the entire building canopy layer. Because PALM discretizes obstacles on a rectilinear grid as mentioned in ~~Sec.~~Section 2.2, smooth building walls are represented by step-wise surfaces if ~~they are~~ not aligned with the grid layout. Therefore, building walls become significantly rougher than they were in the wind-tunnel experiment. This causes higher turbulence and an overall reduced mean wind speed within the building canopy layer.

To better evaluate the deviations between both experiments, we calculated different validation metrics~~were calculated. Within~~ . COST Action 732 (Schatzmann et al., 2010) ~~,~~ lists several validation metrics ~~are listed~~ to help evaluating simulation models. The proposed metrics are the factor-of-two $FAC2$, the hit rate q, the fractional bias FB, the geometric mean bias MG, the normalized mean square error $NMSE$, and the geometric variance VG. Additionally, ~~also~~ we calculated the correlation coefficient

Table 1. Calculated validation metrics for different variables. The right-most column gives the respective value of a perfect match between simulation and observation.

metric	u/u_{ref}	v/u_{ref}	$U_{\text{hor}}/u_{\text{ref}}$	$\sigma_u^2/u_{\text{ref}}^2$	$\sigma_v^2/u_{\text{ref}}^2$	I_u	I_v	ideal
$FAC2$	0.98	0.73	1	0.98	0.98	1	1	1
q	0.91	0.70	0.96	0.82	0.79	0.93	0.91	1
R^2	0.97	0.87	0.96	0.57	0.55	0.83	0.85	1
FB	-	-	0.03	-0.06	0.19	-0.08	0.03	0
MG	-	-	1.05	0.95	1.2	0.93	1.04	1
$NMSE$	-	-	0.01	0.07	0.21	0.05	0.07	0
VG	-	-	1.01	1.05	1.08	1.02	1.02	1
δ_a	0.025	0.025	0.025	0	0	0	0	

R~~is calculated~~. These metrics are defined as:

$$FAC2 = \frac{1}{N}\sum_i n_i \ , \ n_i = \begin{cases} 1 & \text{if } \frac{1}{2} \leq \frac{P_i}{O_i} \leq 2 \ \vee \ (|P_i| \leq \delta_a \wedge |O_i| \leq \delta_a), \\ 0 & \text{otherwise,} \end{cases} \tag{4}$$

$$q = \frac{1}{N}\sum_i n_i \ , \ n_i = \begin{cases} 1 & \text{if } \left|\frac{P_i - O_i}{O_i}\right| \leq \delta_r \ \vee \ |P_i - O_i| \leq \delta_a, \\ 0 & \text{otherwise,} \end{cases} \tag{5}$$

$$R^2 = \left(\frac{1}{N} \frac{1}{\sigma_P \sigma_O} \sum_i (P_i - \overline{P})(O_i - \overline{O}) \right)^2, \tag{6}$$

$$FB = 2\,\frac{\overline{O} - \overline{P}}{\overline{O} + \overline{P}}, \tag{7}$$

$$MG = \exp\left(\overline{\ln(\widetilde{O}_i)} - \overline{\ln(\widetilde{P}_i)} \right) \ \text{ with } \ \widetilde{\varphi} = \max(\varphi, \delta_a), \tag{8}$$

$$NMSE = \frac{1}{N}\sum_i \frac{(P_i - O_i)^2}{\overline{P}\,\overline{O}}, \tag{9}$$

$$VG = \exp\left(\sqrt{\left(\ln(\widetilde{O}_i) - \ln(\widetilde{P}_i) \right)^2} \right) \ \text{ with } \ \widetilde{\varphi} = \max(\varphi, \delta_a), \tag{10}$$

with O_i being the observed (~~wind-tunnel~~wind tunnel), P_i the predicted (PALM) measurements, δ_r the relative deviation threshold, δ_a the absolute deviation threshold, and N the total number of measurements; the overline denotes an average over all measurements and σ_P and σ_O are the standard deviation of P and O, respectively. ~~The deviation thresholds were set~~ We set the deviation thresholds to $\delta_r = 0.25$ for all variables as recommended by VDI (2005)~~and~~ . Table 1 lists the used δ_a ~~as given in Tab. 1~~for all variables.

~~The validation metrics were calculated for the wind velocities u, v and U_{hor}~~We calculated the validation metrics for the horizontal wind speed U_{hor}, the wind-velocity components u and v, their variance σ_u^2 and σ_v^2, ~~and~~ as well as for the turbulence intensities I_u and I_v that are defined as the standard deviation divided by the mean horizontal wind speed ~~. Results are listed~~

~~in~~ (see Tab. 1). In general, all validation metrics are close to their ideal values indicating a ~~very~~ high agreement between both experiments. The largest deviation between both experiments is apparent for v where both $FAC2$ and q give the lowest values. However, q is still within the acceptable range of $q \geq 0.66$, defined by VDI (2005). The metrics also reflect the above-mentioned findings~~of PALM underestimating~~, that PALM underestimates the mean wind speed. Both, FB and MG indicate an ~~about 5 % underestimation ($MG = 1.5$). Also the~~ underestimation of approximately 5 % ($MG = 1.05$). The metrics also indicate an underestimation of σ_v ~~visible in Fig. 10is represented by $MG = 1.2$ indicating about~~ of 20 % ~~lower σ_v for the PALM simulation~~($MG = 1.2$), which is also visible in Figure 10. However, all metrics lie well within the margins reported by Hanna et al. (2004) for an acceptable performing model~~which~~. These margins are $FAC2 > 0.5$, $|FB| < 0.3$, $0.7 < MG < 1.3$, $NMSE < 4$, and $VG < 1.6$.

Hertwig et al. (2017) recommend to ~~also~~ evaluate the shape parameters of the wind speed distributions of u and v when comparing LES and wind-tunnel results. ~~Therefore,~~ Figure 11 shows the skewness γ and the excess kurtosis β ~~are compared and shown in Fig. 11~~of u and v. Between both experiments, γ_u mostly agrees and shows either symmetrical distributions ($\gamma_u \approx 0$) or a positive skew. For v, distributions tend to have a lower skewness in PALM than in the wind-tunnel measurements. Also, β_v is smaller meaning ~~less peaked distributions~~that the distributions are less peaked. This is also related to the higher roughness ~~as~~ in the PALM simulation because this produces a wider spread of the distribution with a less pronounced peak, resulting in lower β and (in case of a positive average as is the case here) γ. Again, this is more pronounced in the span-wise wind component v.

The higher roughness and enhanced turbulence ~~leads~~ lead to a less correlated flow ~~where length scalesare also reduced~~and reduced length scales. Figure 12 displays the comparison of length scales L_u and L_v of the u and v component, respectively. ~~Length scales are calculated~~ We calculated the length scales based on the integral time scale T:

$$L_\varphi = T_\varphi u_{\text{ref}}, \tag{11}$$

where T is calculated using the auto-correlation function R_a:

$$\int_0^{T_\varphi} R_{a,\varphi}(t_l)dt_l = e^{-1} \text{ with } R_{a,\varphi}(t_l) = \frac{1}{\sigma_\varphi^2}\overline{(\varphi(t) - \overline{\varphi}(t))\,(\varphi(t+t_l) - \overline{\varphi}(t+t_l))} \text{ for } \varphi \in \{u, v\}, \tag{12}$$

with t_l being the time lag.

Most striking are the considerably lower values of L_v within the PALM simulation. However, most data points still lie within the factor-of-two margins~~with~~: $FAC2(L_v) = 0.8$. ~~For~~ PALM tends to underestimate low L_u ~~, also lower values tend to be underestimated while higher values tend to be overestimated~~and overestimates L_v.

In the following, we compare ~~vertical profiles of various quantities As many measurement stations~~the vertical profiles recorded at the measurement stations. Because many vertical profiles showed nearly identical behaviour ~~within their vertical profiles~~at different stations, we limit the discussion to three stations: 4, 11, and 7. ~~These are chosen to represent~~ We chose these stations as examples of a good, an average and a relatively poor agreement, respectively, between ~~PALM and~~ the simulation and the wind-tunnel measurements.

Figure 13 shows vertical profiles of U_{hor}, d, u, v, as well as turbulence intensity I, skewness γ, excess kurtosis β and length scale L for u and v measured at station 7. Error bars show the standard deviation of u and v~~measurements~~. The blue shaded area shows the range of values of the neighbouring grid points within PALM at ~~that~~ the respective measurement station.

Station 7 is situated at the opening of a street canyon within the lee of a building edge (see Fig. 3). Because the surrounding building walls ~~are~~ were not aligned with the PALM grid, the building edge ~~has~~ had a different shape within the simulation than ~~it had~~ in the wind-tunnel experiment. This ~~then causes the formation of a slightly~~ shape difference created an enlarged corner vortex ~~. As a result, wind speed is reduced and turbulence increased~~ in the simulation. The vortex increased the turbulence and decreased the mean wind speed at station 7 compared to the wind-tunnel results, as shown in ~~Fig.~~Figure 13. Also, d is affected and deviates from the wind-tunnel results. ~~Above the rooftop, which is situated between 26 m and 36 m in this area~~The effect of rougher building walls by the step-wise representation is limited to the canopy layer. Therefore, d, I_u and I_v agree significantly better to the wind-tunnel measurements ~~, because the effect of rougher building walls is mostly limited to the canopy layer.~~ above the rooftop height, that is situated between 26 m and 36 m in the vicinity of station 7. Due to higher turbulence ~~, also~~ below the rooftop level, β_v ~~is decreased~~ decreases, indicating a less peaked distribution~~while~~ , while the lower γ_u indicates larger tails towards low u values. ~~Higher turbulence due to larger roughness~~ The higher turbulence also causes L to be shorter within the canopy~~as well. The higher roughness introduced by the rougher building walls causes higher vertical momentum flux and hence larger~~ . Above the canopy layer, the mean wind speed and length scales ~~above~~ are larger than in the wind-tunnel experiment because of a higher vertical momentum flux in the simulation, caused by the higher roughness within the canopy layer. Similar behaviour can be found at station 20 (profiles not shown)~~. There, the station is situated closely~~ , which is located close to a windward building corner. In ~~that~~ this case, the blocking effect of the building is increased ~~due to~~ because of the broader building edge, causing significant differences in ~~wind direction~~ wind-direction distribution and mean wind speed (see ~~Fig~~Figs. 8 and 9).

Profiles not affected by corner flows or the blocking effect tend to agree better between PALM and wind-tunnel measurements. Station 11~~is~~ , positioned at the centre of a street canyon (see Fig. 3)~~and profiles~~ , serves as an example of such a measurement location. Profiles tend to agree significantly better within the canopy layer than for station 7, as shown in Fig. 14. Higher deviations between the experiments appear ~~near the building roof level which again is~~ close to the rooftop height (between 26 m and 36 m). The roofs of the surrounding buildings ~~are not flat but~~ have small structures~~which~~ , that might not be sufficiently resolved~~and lead to differences between the experiments. Results at stations~~ . Hence, the details of the building layout differ between the simulation and the wind tunnel at station 11. Stations 5, 6, 10, and 17 ~~are comparable~~ show results similar to those of station 11. ~~Important to note is the large range of values at the surrounding grid points shown~~ Figure 14 shows a large value range of the profiles as indicated by the blue-shaded ~~area within Fig. 14. Profiles vary significantly within a~~ areas. This large range shows that profiles vary significantly inside the street canyon depending on the distance to the building walls. Hence, ~~placing~~ it is very important to place the measurements correctly ~~within the simulation is very important if~~ in the simulation if they are situated in close vicinity to buildings.

~~The less complex the building structures are, the better PALM reproduces the flow of the wind-tunnel experiment.~~ Station 4 is ~~situated~~ located at the leeward site of a ~~fairly simply structured~~ flat-roofed building (see Fig. 3). ~~Profiles~~Also, no building

corners, that could produce blocking effects or corner flows, are within the proximity of station 4. Profiles at station 4, displayed in ~~Fig.~~Figure 15, show ~~nearly no differences~~ only small deviations between the two experiments. ~~Only the influence of the rougher walldue to~~ The rougher wall, generated by the building representation~~is noticeable producing slightly~~ , produces larger turbulence and a less peaked distribution of u and v within the canopy layer. However, results agree significantly better at station 4 compared to station 7 and 11. Hence, PALM reproduces the wind field better if the building structures are less complex.

~~Finally, turbulence spectra in form of the spectral energy density S are compared between PALM and wind-tunnel measurements.~~ Figure 16 shows the ~~dimensionless energy spectra for~~ spectral energy density S measured at station 4 (left panel) and station 11 (right panel) at ~~different heights z.~~ the profile top, rooftop and near the surface (top, centre, and bottom row, respectively). Spectra measured at station 7 are comparable to those of station 11 and are therefore not shown. ~~Note that the~~ The covered range of frequencies f differ between PALM and wind-tunnel measurements~~as~~ , because the sampling rate of the measurements and the measured time interval vary between the PALM and the wind-tunnel experiment. However, results of both experiments ~~still~~ overlap over a large range of frequencies.

~~In general, spectra for~~ Spectra of u and v coincide to a high degree between ~~PALM and~~ the simulation and the wind-tunnel measurements at all heights. ~~The inertial range of the turbulence spectrum is clearly visible within both experiments~~ At both stations, the spectra show an exponential decrease between $\frac{fz}{U_{\mathrm{hor}}} = 2$ and 50 at 75 m height (above the canopy layer)~~at both stations~~ , indicating the inertial range (Figs. 16a and b). The normalized energy spectrum decays with roughly $fS \propto f^{-\frac{2}{3}}$ following Kolmogorov's theory. At high frequencies, spectra of the PALM measurements ~~strongly~~ rapidly decay, which is related to numerical dissipation~~and~~ . This decay is a typical behaviour of LES models using high-order differencing schemes (e.g., Glendening and Haack, 2001; Kitamura and Nishizawa, 2019).

At rooftop height (Figs. 16c and d), PALM's spectra are shifted towards higher frequencies compared to those of the wind tunnel at the same height. ~~Hence,~~ This shift indicates, that PALM simulates smaller-scale turbulence at these heights~~, which might~~ . The shift can be related to higher roughness and further fosters the above-mentioned findings from the profile analysis. The ~~brick-like~~ step-wise representation of the buildings introduces additional roughness causing smaller turbulence elements~~and hence~~ , and hence, a shift of the energy spectrum to higher frequencies. ~~The effect is more pronounced for station 4 than for~~ Station 4 shows a a more pronounced shift than station 11~~which~~, which might, however, ~~might also~~ be related to the more distinct maximum~~and hence~~ , and hence, better visibility of a shift at station 4.

Spectra ~~close to the surface~~ agree better between PALM and the ~~wind tunnel measurements . Though, due to the limited~~ wind-tunnel measurements close to the surface. However, the wind-tunnel measurements did not cover the inertial range at 3 m height, because of the limitation of the measurement frequency and ~~very~~ small turbulent structures ~~at the surface,~~ near the surface. PALM does not resolve the inertial range ~~is not covered by the wind-tunnel measurements at 3 m height. This height corresponds to the third grid level above the surface of the PALM simulation and therefore it can be truly expected that the inertial range is only poorly resolved~~at this height as well, because the turbulence elements are smaller than the grid size of 1 m, hence, the small-scale turbulence cannot be directly simulated. Comparing the measured spectra to the theoretical decay of $f^{-\frac{2}{3}}$, the inertial range is indeed hardly represented within the data.

~~Results within the vicinity of the measurement stations could be improved by utilizing PALM's self-nesting feature (Hellsten et al., 2020) . This allows to use a higher grid resolution within specific areas of the model domain. We recommend that future simulations should try using this feature for areas requiring high resolution.~~

4 Conclusions

In this study, we analyzed PALM's capability to simulate a complex flow field within a realistic urban building array. ~~Simulation results were compared with~~ We compared simulation results to measurements done at the EWTL facility at the University of Hamburg, Germany. The aim was to evaluate the dynamic core of the newest version 6.0 of PALM, which underwent significant code-changes in recent model development.

The comparison of PALM results with the ~~wind tunnel data proves~~ wind-tunnel data demonstrated that PALM is capable ~~to correctly simulate~~ of accurately simulating a neutrally stratified urban boundary layer produced by a realistic, complex building array. ~~Measurements from both experiments were compared at several different~~ We compared measurements from the simulation to those of the wind-tunnel experiment at several positions throughout the building array~~at~~. These positions included non-obstructed locations, ~~at the~~ windward and leeward ~~site of buildingsas well as~~ sides of buildings, within street canyons~~and at~~ , and at roadway intersections. Overall, the PALM results displayed ~~very~~ relatively good agreement with the corresponding wind-tunnel measurements in regards to wind speed and direction, as well as turbulence intensity. Validation metrics ~~as~~ proposed by Schatzmann et al. (2010) were all within the acceptable ~~range~~ranges.

However, ~~it was found that~~ PALM underestimates wind speed and overestimate turbulence close to the ground and building surfaces. ~~Differences were most pronounced~~ Estimates differed most in the span-wise wind velocity component. ~~Such discrepancies were also reported recently by Paas et al. (2020)~~ Paas et al. (2020) recently reported such discrepancies when comparing PALM simulations to real-world measurements. These differences ~~can be ascribed partly~~ occur partly due to an overestimation of roughness mainly introduced by the step-wise representation of ~~the~~ buildings onto PALM's rectilinear grid. This representation causes building walls not aligned with the grid to appear significantly rougher, resulting in lower wind speed and higher turbulence close to walls~~and~~ , especially in the vicinity of building corners. Also, the used roughness length of $z_0 = 0.01\,\mathrm{m}$ might be larger than the actual surface roughness ~~as present~~ in the wind-tunnel experiment, causing the highest difference of mean wind speed (~~$-9\,\%$~~$9\,\%$) at the lowest analysis height.

To a lesser degree, ~~also~~ the miss-match in measurement height is ~~found to be~~ responsible for a difference in mean wind speed. Due to PALM's staggered ~~Arakawa C~~ Arakawa-C grid, output was not available at the exact same position as in the wind-tunnel experiment, but was shifted half a grid spacing ($0.5\,\mathrm{m}$) downwards~~accounting~~ . This half-grid shift accounted for up to $3\,\%$ difference in wind speed at the lowest grid level.

If z_0 is unknown, this can certainly produce differences between PALM and reference data close to surfaces. More importantly, however, is a good representation of building structures. If the focus lies on flow features in close vicinity to buildings, the most important buildings should ~~be aligned~~ align with the simulation grid. Also, we recommend a high grid resolution ~~is recommended~~ to represent structures as close to the reference as possible. To achieve this, future validations

could utilize PALM's nesting feature ~~could be utilized~~ in order to cope with increasing computational demand ~~if the grid size is reduced~~ of reduced grid size (Hellsten et al., 2020). A higher resolution ~~has the additional benefit of reducing~~ also reduces the errors introduced by shifting locations of measurements ~~if PALM results are compared~~ of PALM when comparing against reference data~~which otherwise can~~. These errors can otherwise cause deviations close to ~~building structures~~ buildings, where large gradients can ~~lead to~~ cause significant differences in results (~~as can be seen~~see, e.g., ~~by the range of profiles at~~ profiles of station 11, Fig. 14). In a future release of PALM, an immersed boundary condition ~~is going to be available (Mittal and Iaccarino, 2005, e.g.). This will then~~ will be available (e.g. Mittal and Iaccarino, 2005). This new boundary condition will mitigate the increased roughness effect introduced by the step-wise representation of building walls not aligned with the rectilinear grid.

Lastly, we ~~would like to give~~ provide some general advice for the setup preparation. In the present study, we experienced that input data must always be checked with very high caution~~. Especially~~, especially large building data sets. These building setups might contain errors and false building heights or missing/displaced buildings, which are more difficult to spot than in setups with a limited number of buildings. This is, of course, of utmost importance for the area of interest~~, but also~~. However, the upwind region also requires proper verification ~~as~~ because it directly affects the analysis area. ~~Also~~Additionally, when comparing to other experiments, like real-world or wind-tunnel measurements, positioning of the measurements must be thoroughly checked, as mentioned by Paas et al. (2020). This is ~~also~~ true for positioning virtual measurements within the PALM domain, as well. At positions with ~~highly~~ complex wind fields, it can make a large difference for the results if measurement positions are off by only a single grid point. This of course depends ~~strongly~~ on the grid spacing ~~used~~ and will be most relevant when using relatively coarse grids.

This study focused ~~only on a single~~ on only a single, but the most essential~~part~~, component of PALM, the dynamic core. However, a full validation of the entire model requires additional studies focusing on the other model ~~parts~~ components like the radiation module, the chemistry module or the land-surface module~~to mention only a few~~. Some of these are already validated (Resler et al., 2017; Kurppa et al., 2019; Fröhlich and Matzarakis, 2019; Gehrke et al., 2020)~~, others~~. Others will follow in future publications.

Code and data availability. The PALM model system is freely available from http://palm-model.org and distributed under the GNU General Public License v3 (http://www.gnu.org/copyleft/gpl.html). The model source code of version 6.0 in revision 3921, used in this article, is archived on the Research Data Repository of the Leibniz University of Hannover (Gronemeier et al., 2020b) as well as input data and measurement results presented in this paper, together with the plotting scripts to reproduce the presented figures (Gronemeier et al., 2020a).

Author contributions. BL and KS created the wind-tunnel setup. KS conducted the wind-tunnel measurements and analysis with supervision of FH and BL. TG, SR and BM created the simulation setup. TG carried out the simulations and precursor test simulations with supervision of SR. All authors took part in data analysis of the comparison. TG compiled the manuscript with contributions by all coauthors.

Competing interests. The authors declare that no competing interests are present.

Acknowledgements. We like to thank everyone who helped to conduct the experiments and helped by writing software for the analysis of the results (including data preparation, model building, and code bug-fixing). We ~~also like to thank the~~ thank the two anonymous referees who helped to significantly improve the script with their valuable comments. We thank Wieke Heldens and Julian Zeidler (German Aerospace Center, DLR) for the support during the project and especially for preparing the building data used within this study. We thank Christopher Mount (Leibniz University Hannover) for proofreading the manuscript. This study was part of the [UC]^2 project that is funded by the German Federal Ministry of Education and Research (BMBF) within the framework 'Research for Sustainable Development' (FONA; www.fona.de). ~~It~~ The study was conducted in collaboration of the two sub-projects MOSAIK (funding code: 01LP1601) and 3DO (funding code: 01LP1602)~~. The authors would like to thank Wieke Heldens and Julian Zeidler at the German Aerospace Center (DLR) for the support during the project and especially for preparing the building data used within this study~~. All simulations were carried out on the computer clusters of the North-German Supercomputing Alliance (HLRN; www.hlrn.de). Data analysis was done using Python.

References

Arakawa, A. and Lamb, V. R.: Computational Design of the Basic Dynamical Processes of the UCLA General Circulation Model, in: General Circulation Models of the Atmosphere, vol. 17, pp. 173–265, Methods in computational Physics, edited by: Chang, J., 1977.

Basu, S. and Lacser, A.: A Cautionary Note on the Use of Monin–Obukhov Similarity Theory in Very High-Resolution Large-Eddy Simulations, Boundary-Layer Meteorol, 163, 351–355, https://doi.org/10.1007/s10546-016-0225-y, 2017.

Blocken, B.: Computational Fluid Dynamics for Urban Physics: Importance, Scales, Possibilities, Limitations and Ten Tips and Tricks towards Accurate and Reliable Simulations, Building and Environment, 91, 219–245, https://doi.org/10.1016/j.buildenv.2015.02.015, 2015.

Blocken, B., Carmeliet, J., and Stathopoulos, T.: CFD Evaluation of Wind Speed Conditions in Passages between Parallel Buildings—Effect of Wall-Function Roughness Modifications for the Atmospheric Boundary Layer Flow, Journal of Wind Engineering and Industrial Aerodynamics, 95, 941–962, https://doi.org/10.1016/j.jweia.2007.01.013, 2007.

Briscolini, M. and Santangelo, P.: Development of the Mask Method for Incompressible Unsteady Flows, J. Comp. Phys., 84, 57–75, https://doi.org/10.1016/0021-9991(89)90181-2, 1989.

Fröhlich, D. and Matzarakis, A.: Calculating Human Thermal Comfort and Thermal Stress in the PALM Model System 6.0, Geosci. Model Dev. Discuss., 2019, 1–21, https://doi.org/10.5194/gmd-2019-202, in review, 2019.

Gehrke, K. F., Sühring, M., and Maronga, B.: Modeling of Land-Surface Interactions in the PALM Model System 6.0: Land Surface Model Description, First Evaluation, and Sensitivity to Model Parameters, Geosci Model Dev Discuss, 2020, https://doi.org/10.5194/gmd-2020-197, 2020.

Glendening, J. W. and Haack, T.: Influence Of Advection Differencing Error Upon Large-Eddy Simulation Accuracy, Boundary-Layer Meteorol, 98, 127–153, https://doi.org/10.1023/A:1018734205850, 2001.

Gronemeier, T. and Sühring, M.: On the Effects of Lateral Openings on Courtyard Ventilation and Pollution—A Large-Eddy Simulation Study, Atmosphere, 10, 63, https://doi.org/10.3390/atmos10020063, 2019.

Gronemeier, T., Surm, K., Harms, F., Leitl, B., Maronga, B., and Raasch, S.: Dataset: Evaluation of the Dynamic Core of the PALM Model System 6.0 in a Neutrally Stratified Urban Environment: Simulation Input Data and Measurement Data., https://doi.org/10.25835/0015082, 2020a.

Gronemeier, T. et al.: Dataset: PALM 6.0 r3921, https://doi.org/10.25835/0046914, 2020b.

Hanna, S. R., Hansen, O. R., and Dharmavaram, S.: FLACS CFD Air Quality Model Performance Evaluation with Kit Fox, MUST, Prairie Grass, and EMU Observations, Atmos. Environ., 38, 4675–4687, https://doi.org/10.1016/j.atmosenv.2004.05.041, 2004.

Harlow, F. H. and Welch, J. E.: Numerical Calculation of Time-Dependent Viscous Incompressible Flow of Fluid with Free Surface, Phys. Fluids, 8, 2182, https://doi.org/10.1063/1.1761178, 1965.

Hellsten, A., Ketelsen, K., Sühring, M., Auvinen, M., Maronga, B., Knigge, C., Barmpas, F., Tsegas, G., Moussiopoulos, N., and Raasch, S.: A Nested Multi-Scale System Implemented in the Large-EddySimulation Model PALM Model System 6.0, Geosci. Model Dev Discuss, 2020, 1–45, https://doi.org/10.5194/gmd-2020-222, 2020.

Hertwig, D., Patnaik, G., and Leitl, B.: LES Validation of Urban Flow, Part I: Flow Statistics and Frequency Distributions, Environ Fluid Mech, 17, 521–550, https://doi.org/10.1007/s10652-016-9507-7, 2017.

Kanda, M., Inagaki, A., Miyamoto, T., Gryschka, M., and Raasch, S.: A New Aerodynamic Parametrization for Real Urban Surfaces, Boundary-Layer Meteorol, 148, 357–377, https://doi.org/10.1007/s10546-013-9818-x, 2013.

Kitamura, Y. and Nishizawa, S.: Estimation of Energy Dissipation Caused by Odd Order Difference Schemes for an Unstable Planetary Boundary Layer, Atmos Sci Lett, 20, e905, https://doi.org/10.1002/asl.905, 2019.

Kurppa, M., Hellsten, A., Auvinen, M., Raasch, S., Vesala, T., and Järvi, L.: Ventilation and Air Quality in City Blocks Using Large-Eddy Simulation—Urban Planning Perspective, Atmosphere, 9, 65, https://doi.org/10.3390/atmos9020065, 2018.

Kurppa, M., Hellsten, A., Roldin, P., Kokkola, H., Tonttila, J., Auvinen, M., Kent, C., Kumar, P., Maronga, B., and Järvi, L.: Implementation of the Sectional Aerosol Module SALSA2.0 into the PALM Model System 6.0: Model Development and First Evaluation, Geosci. Model Dev., 12, 1403–1422, https://doi.org/10.5194/gmd-12-1403-2019, 2019.

Leitl, B. and Schatzmann, M.: Validation Data for Urban Flow and Dispersion Models - Are Wind Tunnel Data Qualified?, in: The Fifth International Symposium on Computational Wind Engineering (CWE2010), p. 8, Chapel Hill, North Carolina, USA, 2010.

Letzel, M. O., Krane, M., and Raasch, S.: High Resolution Urban Large-Eddy Simulation Studies from Street Canyon to Neighbourhood Scale, Atmospheric Environment, 42, 8770–8784, https://doi.org/10.1016/j.atmosenv.2008.08.001, 2008.

Letzel, M. O., Helmke, C., Ng, E., An, X., Lai, A., and Raasch, S.: LES Case Study on Pedestrian Level Ventilation in Two Neighbourhoods in Hong Kong, Meteorol. Z., 21, 575–589, https://doi.org/10.1127/0941-2948/2012/0356, 2012.

Li, S., Jaroszynski, S., Pearse, S., Orf, L., and Clyne, J.: VAPOR: A Visualization Package Tailored to Analyze Simulation Data in Earth System Science, Atmosphere, 10, https://doi.org/10.3390/atmos10090488, 2019.

Maronga, B., Gryschka, M., Heinze, R., Hoffmann, F., Kanani-Sühring, F., Keck, M., Ketelsen, K., Letzel, M. O., Sühring, M., and Raasch, S.: The Parallelized Large-Eddy Simulation Model (PALM) Version 4.0 for Atmospheric and Oceanic Flows: Model Formulation, Recent Developments, and Future Perspectives, Geosci. Model Dev., 8, 2515–2551, https://doi.org/10.5194/gmd-8-2515-2015, 2015.

Maronga, B., Gross, G., Raasch, S., Banzhaf, S., Forkel, R., Heldens, W., Kanani-Sühring, F., Matzarakis, A., Mauder, M., Pavlik, D., Pfafferott, J., Schubert, S., Seckmeyer, G., Sieker, H., and Winderlich, K.: Development of a New Urban Climate Model Based on the Model PALM – Project Overview, Planned Work, and First Achievements, Meteorol. Z., 28, 105–119, https://doi.org/10.1127/metz/2019/0909, 2019.

Maronga, B., Banzhaf, S., Burmeister, C., Esch, T., Forkel, R., Fröhlich, D., Fuka, V., Gehrke, K. F., Geletič, J., Giersch, S., Gronemeier, T., Groß, G., Heldens, W., Hellsten, A., Hoffmann, F., Inagaki, A., Kadasch, E., Kanani-Sühring, F., Ketelsen, K., Khan, B. A., Knigge, C., Knoop, H., Krč, P., Kurppa, M., Maamari, H., Matzarakis, A., Mauder, M., Pallasch, M., Pavlik, D., Pfafferott, J., Resler, J., Rissmann, S., Russo, E., Salim, M., Schrempf, M., Schwenkel, J., Seckmeyer, G., Schubert, S., Sühring, M., von Tils, R., Vollmer, L., Ward, S., Witha, B., Wurps, H., Zeidler, J., and Raasch, S.: Overview of the PALM Model System 6.0, Geosci. Model Dev., 13, 1335–1372, https://doi.org/10.5194/gmd-13-1335-2020, 2020a.

Maronga, B., Knigge, C., and Raasch, S.: An Improved Surface Boundary Condition for Large-Eddy Simulations Based on Monin-Obukhov Similarity Theory: Evaluation and Consequences for Grid Convergence in Neutral and Stable Conditions, Boundary-Layer Meteorol, 174, 297–325, https://doi.org/10.1007/s10546-019-00485-w, 2020b.

Mittal, R. and Iaccarino, G.: Immersed Boundary Methods, Annu. Rev. Fluid Mech., 37, 239–261, https://doi.org/10.1146/annurev.fluid.37.061903.175743, 2005.

Munters, W., Meneveau, C., and Meyers, J.: Shifted Periodic Boundary Conditions for Simulations of Wall-Bounded Turbulent Flows, Physics of Fluids, 28, 025 112, https://doi.org/10.1063/1.4941912, 2016.

Oberkampf, W. L., Trucano, T. G., and Hirsch, C.: Verification, Validation, and Predictive Capability in Computational Engineering and Physics, Applied Mechanics Reviews, 57, 345–384, https://doi.org/10.1115/1.1767847, 2004.

Paas, B., Zimmermann, T., and Klemm, O.: Analysis of a Turbulent Wind Field in a Street Canyon: Good Agreement between LES Model Results and Data from a Mobile Platform, Meteorol. Z., p. 93256, https://doi.org/10.1127/metz/2020/1006, 2020.

Park, S.-B., Baik, J.-J., Raasch, S., and Letzel, M. O.: A Large-Eddy Simulation Study of Thermal Effects on Turbulent Flow and Dispersion in and above a Street Canyon, J. Appl. Meteor. Climatol., 51, 829–841, https://doi.org/10.1175/JAMC-D-11-0180.1, 2012.

Park, S.-B., Baik, J.-J., and Lee, S.-H.: Impacts of Mesoscale Wind on Turbulent Flow and Ventilation in a Densely Built-up Urban Area, J. Appl. Meteor. Climatol., 54, 811–824, https://doi.org/10.1175/JAMC-D-14-0044.1, 2015.

Razak, A. A., Hagishima, A., Ikegaya, N., and Tanimoto, J.: Analysis of Airflow over Building Arrays for Assessment of Urban Wind Environment, Building and Environment, 59, 56–65, https://doi.org/10.1016/j.buildenv.2012.08.007, 2013.

Resler, J., Krč, P., Belda, M., Juruš, P., Benešová, N., Lopata, J., Vlček, O., Damašková, D., Eben, K., Derbek, P., Maronga, B., and Kanani-Sühring, F.: PALM-USM v1.0: A New Urban Surface Model Integrated into the PALM Large-Eddy Simulation Model, Geosci. Model Dev., 10, 3635–3659, https://doi.org/10.5194/gmd-10-3635-2017, 2017.

Schatzmann, M., Olesen, H., and Franke, J., eds.: COST 732 Model Evaluation Case Studies: Approach and Results, University of Hamburg, Hamburg, Germany, 2010.

Scherer, D., Antretter, F., Bender, S., Cortekar, J., Emeis, S., Fehrenbach, U., Gross, G., Halbig, G., Hasse, J., Maronga, B., Raasch, S., and Scherber, K.: Urban Climate Under Change [UC]2 – A National Research Programme for Developing a Building-Resolving Atmospheric Model for Entire City Regions, Meteorol. Z., 28, 95–104, https://doi.org/10.1127/metz/2019/0913, 2019.

VDI: Environmental Meteorology – Prognostic Microscale Windfield Models – Evaluation for Flow around Buildings and Obstacles, Tech. Rep. VDI 3783 Part 9, VDI/DIN-Kommission Reinhaltung der Luft (KRdL) - Normenausschuss, 2005.

Wang, W. and Ng, E.: Air Ventilation Assessment under Unstable Atmospheric Stratification — A Comparative Study for Hong Kong, Building and Environment, 130, 1–13, https://doi.org/10.1016/j.buildenv.2017.12.018, 2018.

Wicker, L. J. and Skamarock, W. C.: Time-Splitting Methods for Elastic Models Using Forward Time Schemes, MONTHLY WEATHER REVIEW, 130, 10, 2002.

Williamson, J.: Low-Storage Runge-Kutta Schemes, Journal of Computational Physics, 35, 48–56, https://doi.org/10.1016/0021-9991(80)90033-9, 1980.

Figure 1. Photograph of the building setup within the wind-tunnel facility 'WOTAN' for an approaching flow of 290°. Please note that contrary to the depicted orientation, an approaching flow from 110° was used within this study.

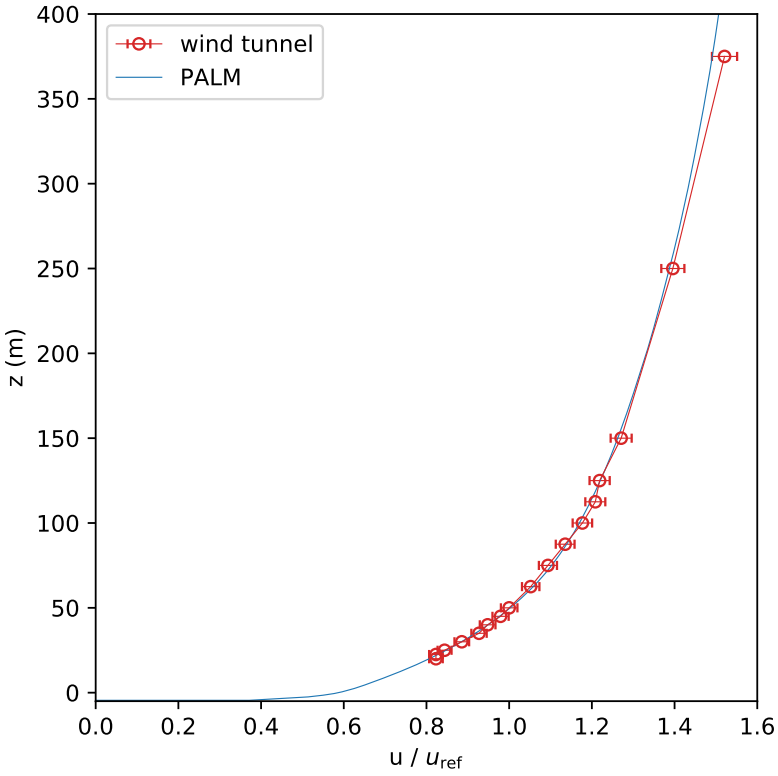

Figure 2. Mean profiles of the approaching flow for the wind-tunnel experiment and the PALM simulation normalized with the reference velocity $u_{\mathrm{ref}} = u(z = 50\,\mathrm{m})$. Note that $z = 0\,\mathrm{m}$ is defined at street-level height while the lowest level within both experiments was at $z = -5\,\mathrm{m}$, which is the water-level height.

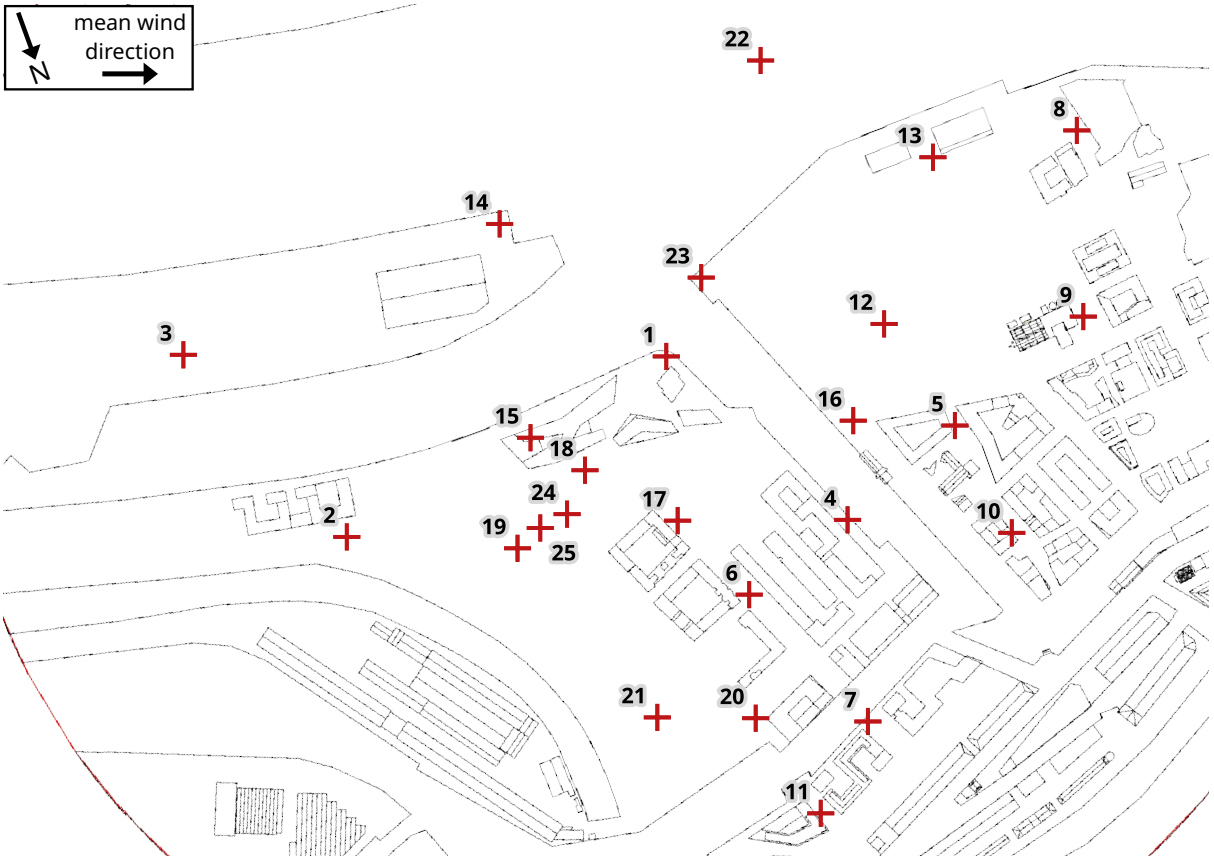

Figure 3. Building layout used in the wind-tunnel experiment. Measurement locations are marked and labeled by their respective number.

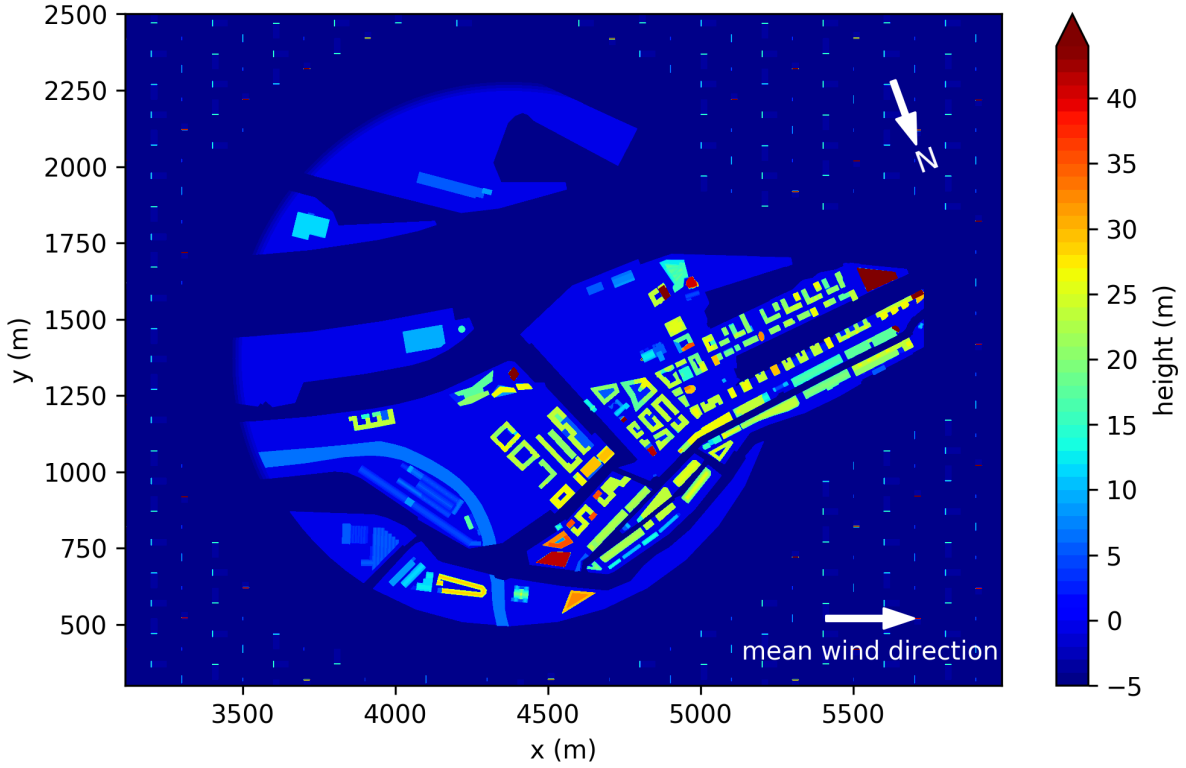

Figure 4. Building layout and heights as used in the PALM simulation. The x-direction is oriented to follow the mean wind direction. The total domain size is $6000\,\mathrm{m}$, $2880\,\mathrm{m}$, and $601\,\mathrm{m}$ in x-, y-, and z-direction, respectively. Note that $z = 0\,\mathrm{m}$ is defined at street-level height while the lowest level within both experiments was at $z = -5\,\mathrm{m}$, which is the water-level height.

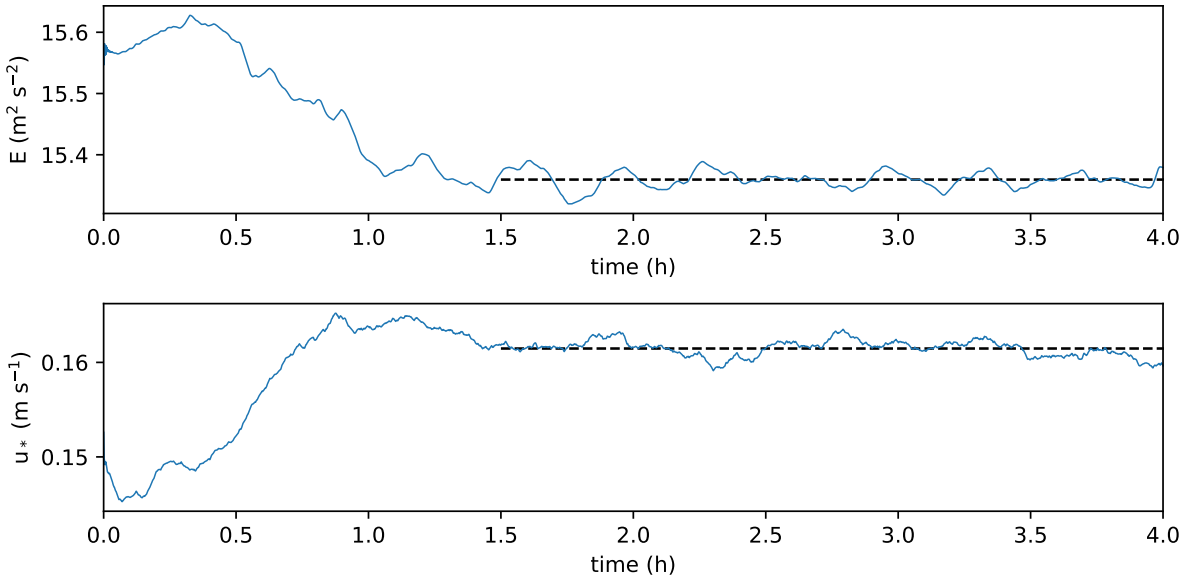

Figure 5. Time series of the total kinetic energy E and the friction velocity u_* of the PALM simulation.

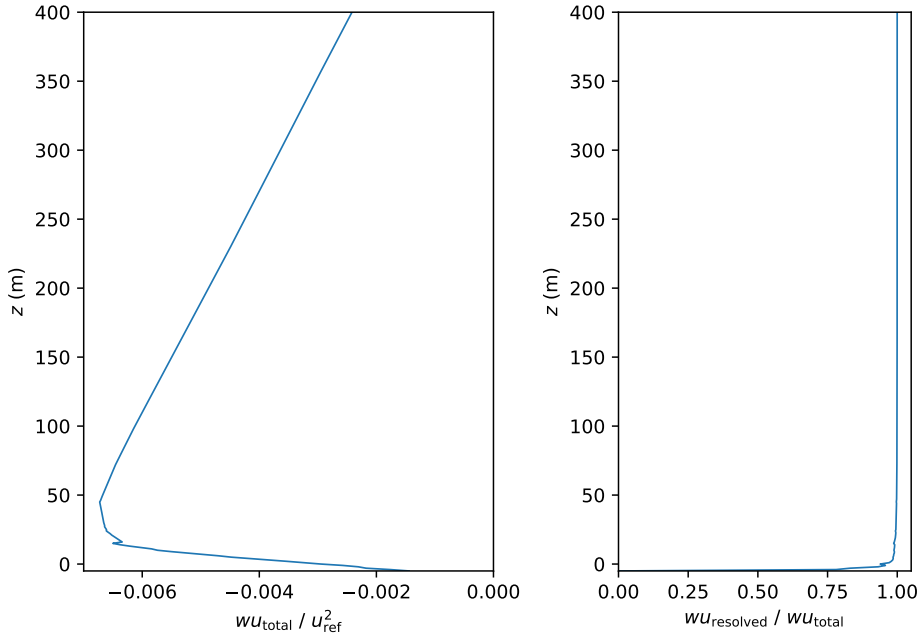

Figure 6. Mean profile of the vertical momentum flux and the ratio between resolved and total flux, averaged over the entire domain of the PALM simulation. Please note the two different horizontal scales for momentum flux (bottom scale) and flux ratio (top scale).

Figure 7. View of the volume-rendered instantaneous turbulence structures above the building array. Turbulence is visualized using the magnitude of the three-dimensional vorticity. Green and red colour show low and high values, respectively. Image was rendered using VAPOR (Li et al., 2019, www.vapor.ucar.edu), the background image was designed by freepic.diller / Freepik (http://www.freepik.com).

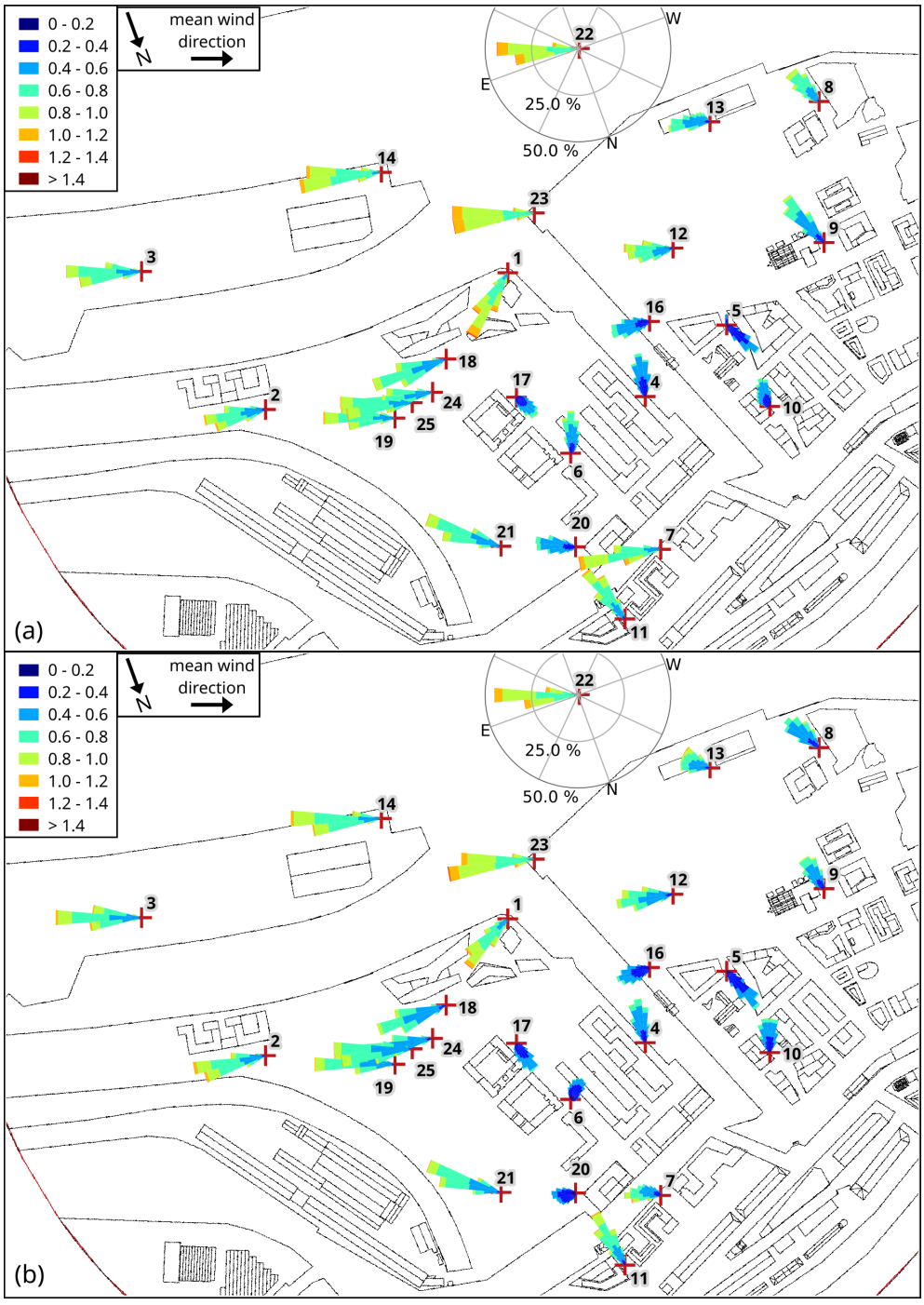

Figure 8. Wind-speed distribution (wind rose plots) at all measurement stations for (a) wind-tunnel measurements and (b) the PALM simulation at about 3 m height above street level (wind tunnel: 3 m, PALM: 2.5 m). Axes are only shown for a single station for better overview, but all wind distributions are scaled equal. Numbers indicate the station number.

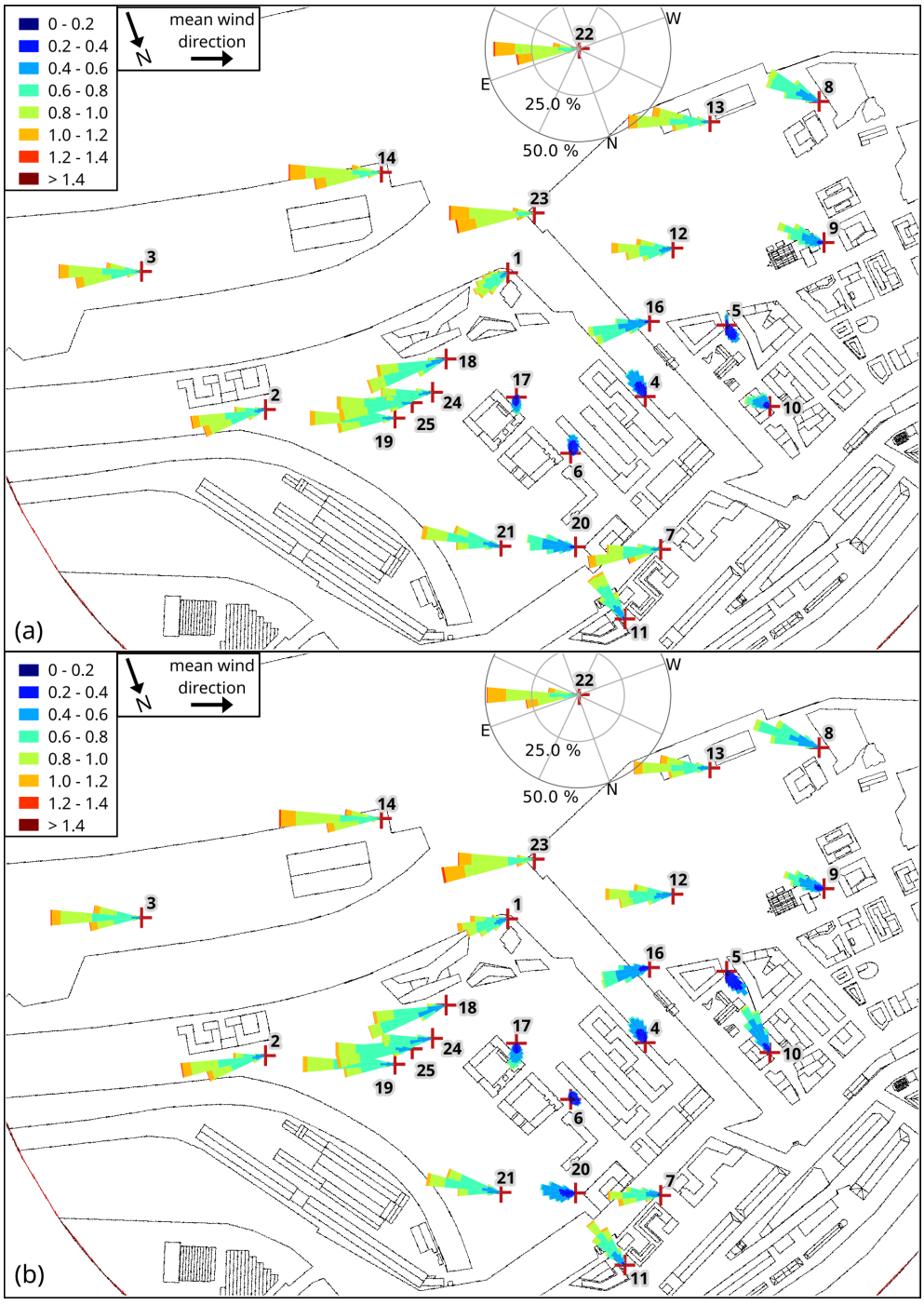

Figure 9. Wind-speed distribution (wind rose plots) at all measurement stations for (a) wind-tunnel measurements and (b) the PALM simulation at about 10 m height above street level (wind tunnel: 10 m, PALM: 9.5 m). Axes are only shown for a single station for better overview, but all wind distributions are scaled equal. Numbers indicate the station number.

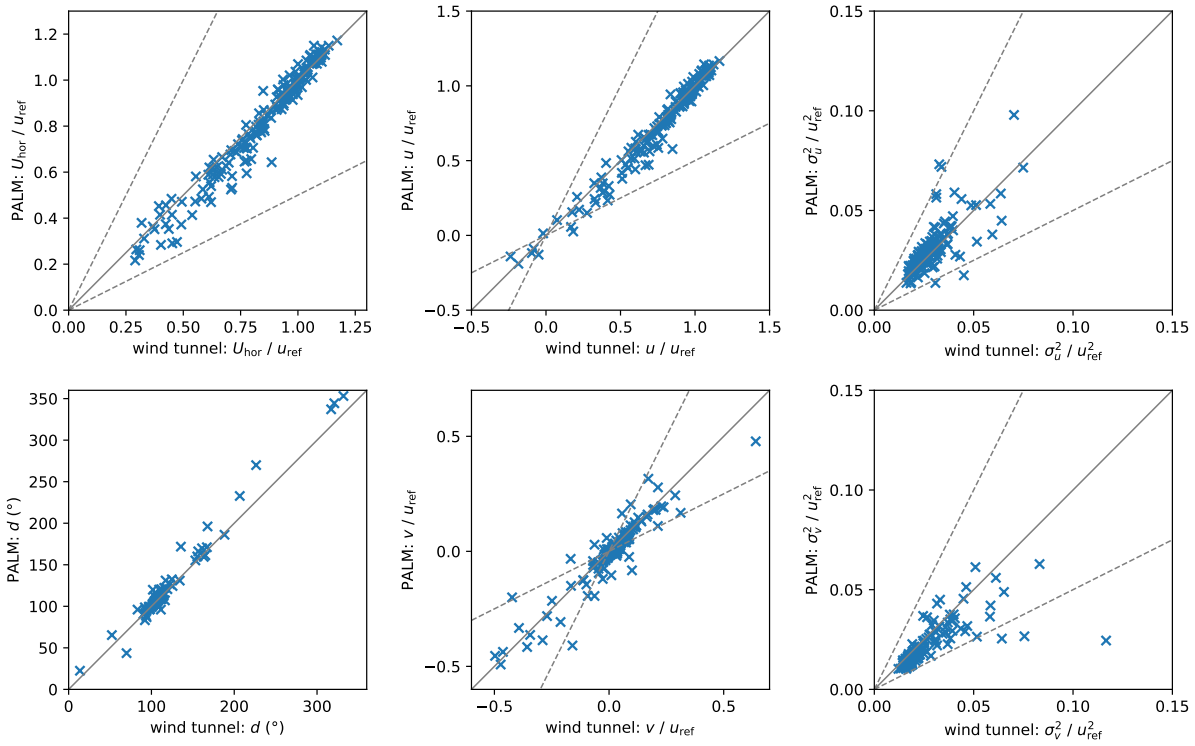

Figure 10. Scatter plots of wind tunnel and PALM measurements of horizontal wind speed U_{hor}, wind direction d, wind-velocity components u and v, and their variance σ_u^2 and σ_v^2 for all 25 measurement stations and all heights (173 data pairs in total). Solid lines indicate perfect agreement, dashed lines indicate the area between a deviation factor of 0.5 and 2.

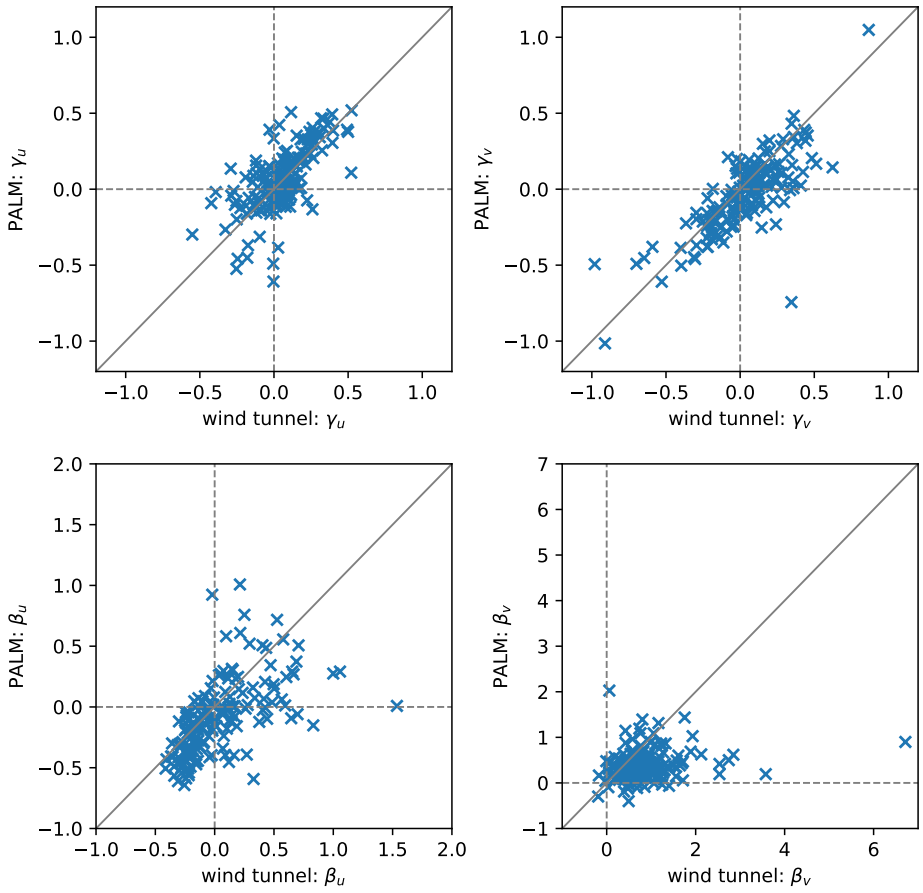

Figure 11. Scatter plots of wind tunnel and PALM measurements of skewness γ and excess kurtosis β of the horizontal wind velocity components for all 25 measurement stations and all heights (173 data pairs in total). Solid lines indicate perfect agreement.

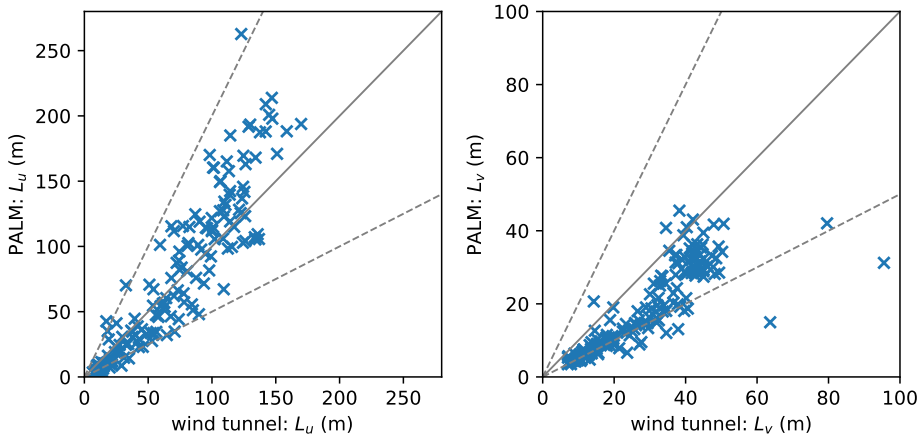

Figure 12. Scatter plots of wind tunnel and PALM measurements of the length scales L_u and L_v of the velocity components u and v, respectively, for all 25 measurement stations and all heights (173 data pairs in total). Solid lines indicate perfect agreement, dashed lines indicate the area between a deviation factor of 0.5 and 2.

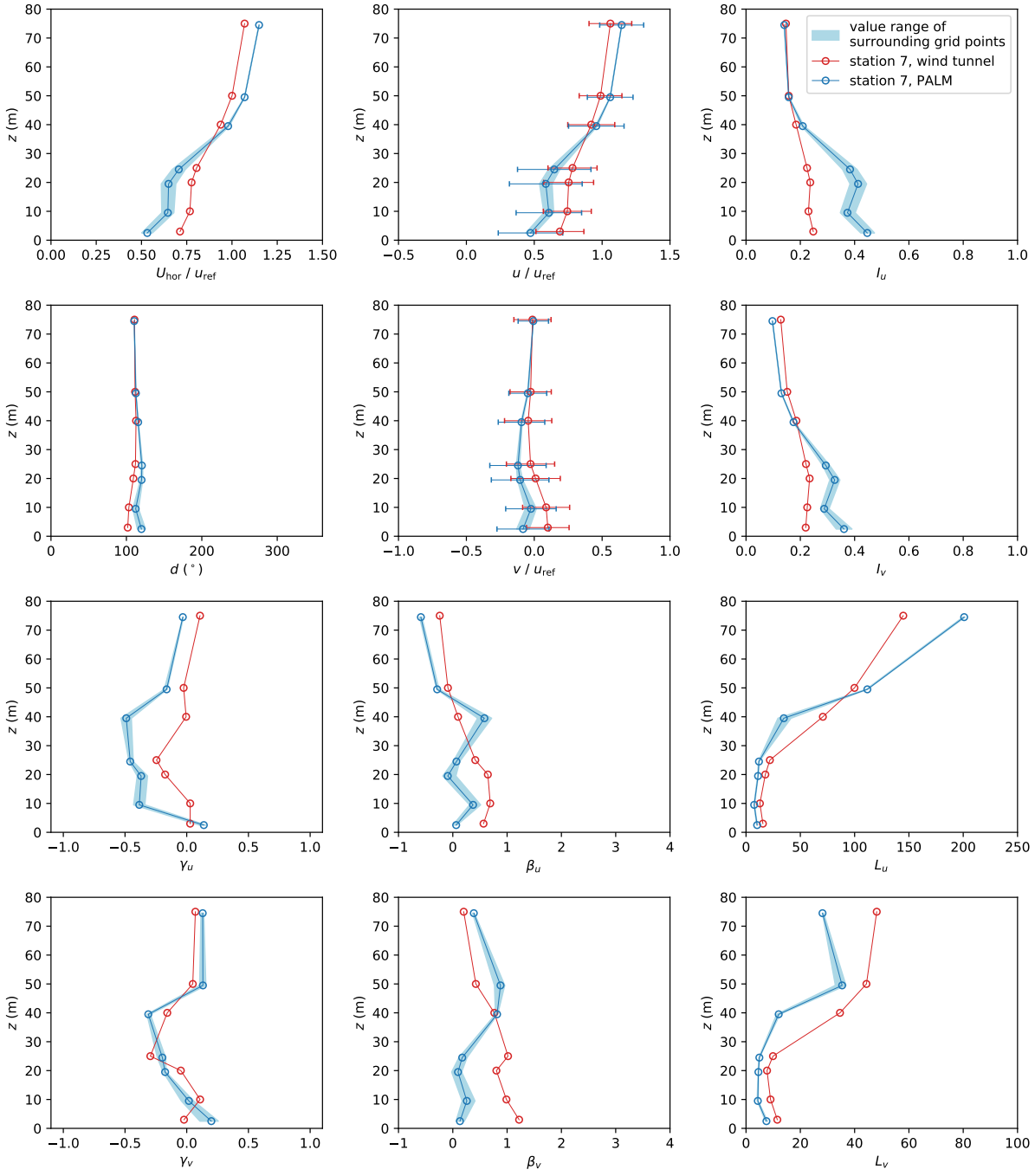

Figure 13. Profiles of mean horizontal wind speed U_{hor}, wind direction d, wind components u and v, as well as turbulence intensity I, skewness γ, excess kurtosis β and length scale L of both wind velocity components u and v at measurement station 7. Error bars denote the standard deviation of the respective quantity. Note that $z = 0$ denotes street-level height.

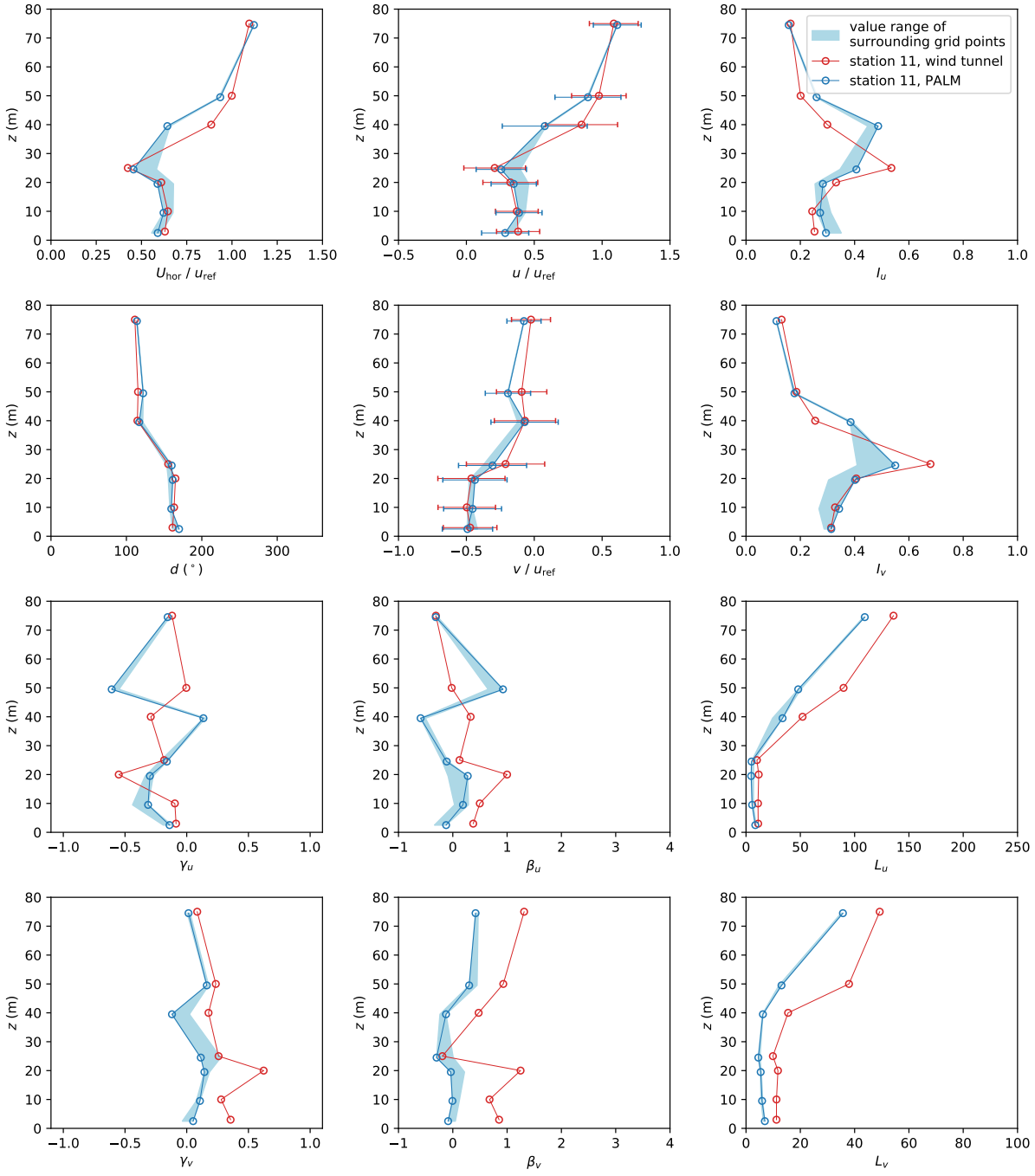

Figure 14. Profiles of mean horizontal wind speed U_{hor}, wind direction d, wind components u and v, as well as turbulence intensity I, skewness γ, excess kurtosis β and length scale L of both wind velocity components u and v at measurement station 11. Error bars denote the standard deviation of the respective quantity. Note that $z = 0$ denotes street-level height.

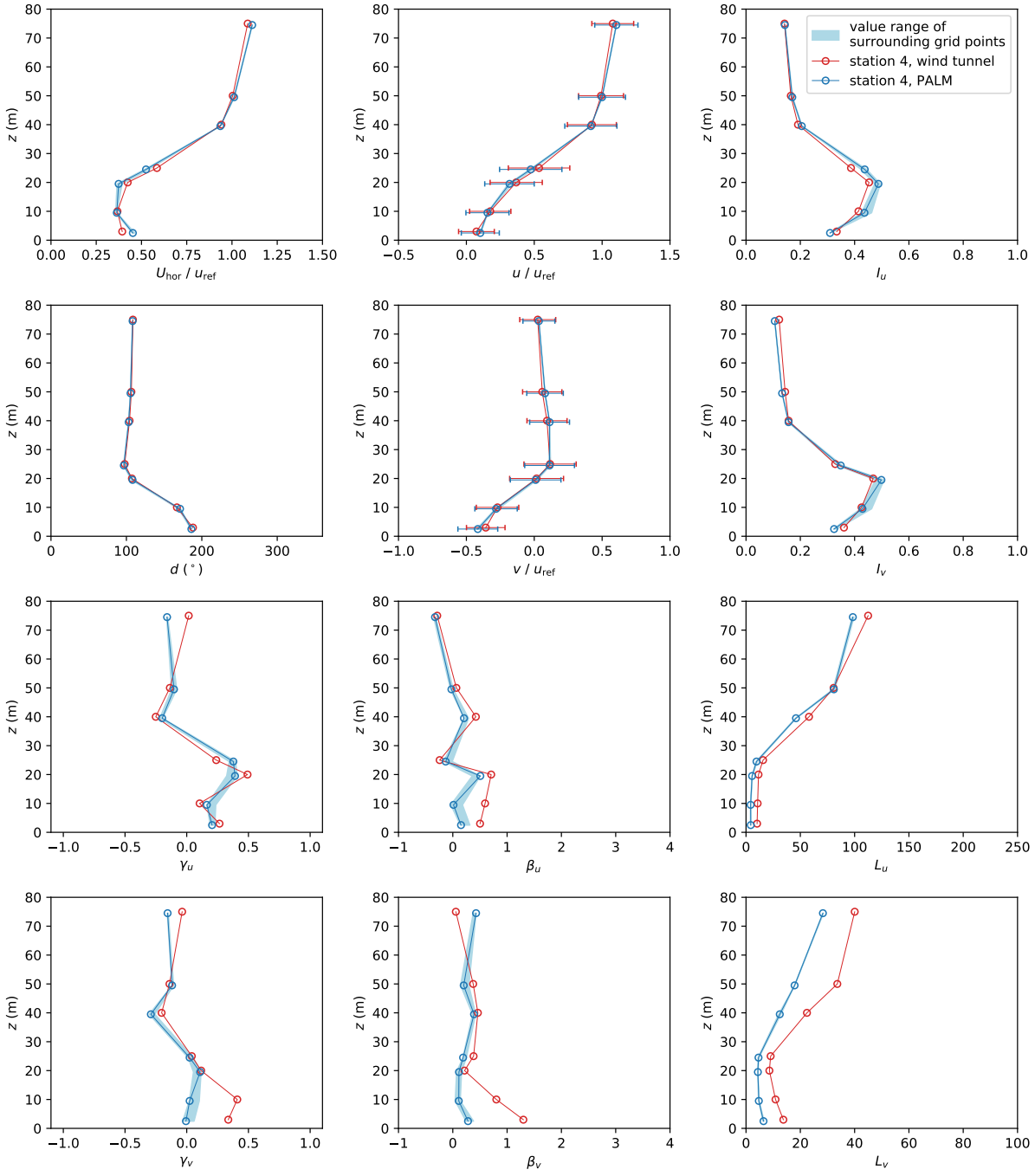

Figure 15. Profiles of mean horizontal wind speed U_{hor}, wind direction d, wind components u and v, as well as turbulence intensity I, skewness γ, excess kurtosis β and length scale L of both wind velocity components u and v at measurement station 4. Error bars denote the standard deviation of the respective quantity. Note that $z = 0$ denotes street-level height.

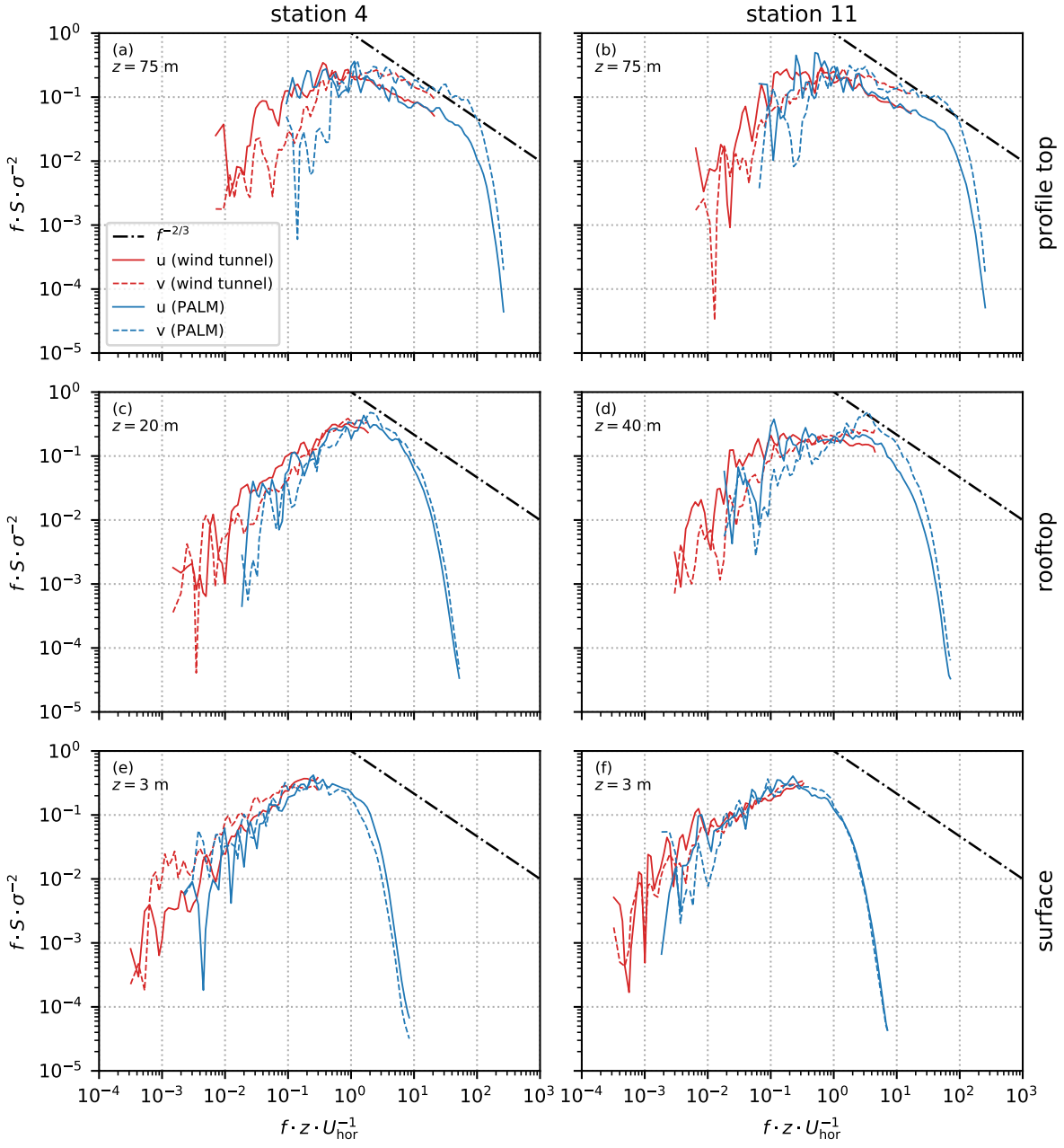

Figure 16. Spectral energy density S for u and v at station 4 (left) and station 11 (right) at profile top (a, b), rooftop height (c, d), and near the surface (e, f). S is normalized by multiplying with the frequency f and dividing by the variance σ^2. For reference, the dash-dotted line shows a slope $f^{-\frac{2}{3}}$ indicating the slope of energy decay according to Kolmogorov's theory. Note that z is given relative to street-level height.